LANGMUIR

Invited Feature Article

pubs.acs.org/Langmuir

Kinetics of Wetting and Spreading of Droplets over Various Substrates

Omid Arjmandi-Tash,[†] Nina M. Kovalchuk,[†,‡] Anna Trybala,[†] Igor V. Kuchin,[†,§] and Victor Starov*[,†]

[†]Deparment of Chemical Engineering, Loughborough University, Loughborough LE11 3TU, U.K.

[‡]Institute of Biocolloid Chemistry, Kiev 03142, Ukraine

[§]Institute of Physical Chemistry and Electrochemistry RAS, Moscow 119071, Russia

ABSTRACT: There has been a substantial increase in the number of publications in the field of wetting and spreading since 2010. This increase in the rate of publications can be attributed to the broader application of wetting phenomena in new areas. It is impossible to review such a huge number of publications; that is, some topics in the field of wetting and spreading are selected to be discussed below. These topics are as follows: (i) Contact angle hysteresis on smooth homogeneous solid surfaces via disjoining/conjoining pressure. It is shown that the hysteresis contact angles can be calculated via disjoining/conjoining pressure. The theory indicates that the equilibrium contact angle is closer to a static receding contact angle than to a static advancing contact angle. (ii) The wetting of deformable substrates, which is caused by surface forces action in the vicinity of the apparent three-phase contact line, leading to a deformation on the substrate. (iii) The kinetics of wetting and spreading of non-Newtonian liquid (blood) over porous substrates. We showed that in spite of the enormous complexity of blood, the spreading over porous substrate can be described using a relatively simple model: a power low-shear-thinning non-Newtonian liquid. (iv) The kinetics of spreading of surfactant solutions. In this part, new results related to various surfactant solution mixtures (synergy and crystallization) are discussed, which shows some possible direction for the future revealing of superspreading phenomena. (v) The kinetics of spreading of surfactant solutions over hair. Fundamental problems to be solved are identified.

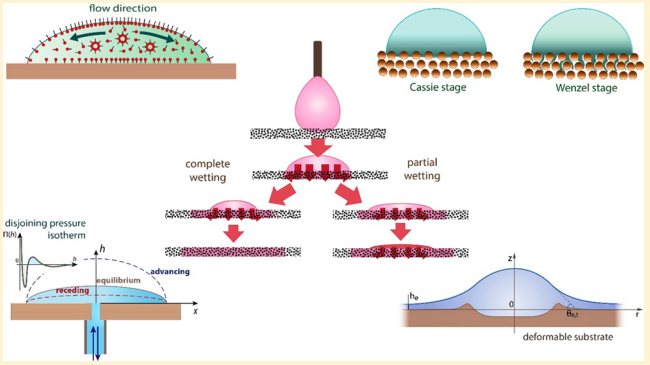

INTRODUCTION

The interest in wetting and spreading phenomena has increased considerably in the last two decades, especially since 2010. According to the ACS and ScienceDirect, altogether around 526 000 papers have been published since 1994 under the keyword wetting. The growth rate of the number of publications increased considerably since 2010 after approximately linear growth during 1998−2010. This increase in the rate of publications corresponds to the broader application of wetting phenomena in new fields: medicine, biology, and various environmental and engineering applications. Our group has been involved in investigations of wetting and spreading phenomena for more than three decades, including a substantial collaboration with industry. The latter determines the selection of topics to be discussed below.

Some basic definitions in the wetting and spreading area are briefly described before starting the discussion. It is usually believed that after the deposition of a droplet on a solid substrate the droplet reaches an equilibrium contact angle after a period of time from the deposition (no matter what the vapor pressure is). Unfortunately, this is in contradiction to thermodynamics: according to the Laplace equation, the convex surface of the droplet means that the pressure inside the droplet is higher than the surrounding pressure in the vapor/air. In its turn, this means that the droplet can be at equilibrium according to Kelvin's equation (eq 6) with oversaturated vapor only. It is shown in ref 1 that the equilibrium conditions are even more restrictive and hardly achievable under regular experimental conditions. This means that after deposition the droplets achieve a contact angle that is different from equilibrium and usually is referred to as the static advancing contact angle.[1] If the liquid from the droplet is drawn off of the droplet, then the droplet will not start receding but will stay until some critical contact angle is reached, the so-called static receding contact angle.[1] In the region close to the apparent three-phase contact line, some new forces take action:[1,2] surface forces or disjoining/conjoining pressure. It is well known that the equilibrium contact angle can be calculated via the disjoining/conjoining pressure isotherm according to the Derjaguin−Frumkin equation.[2] However, the equilibrium contact angle (as explained above) is difficult, if possible at all, to be observed experimentally, and only static advancing and static receding contact angles can be determined, which are referred to as hysteresis contact angles. Is it possible to calculate both

Received: November 11, 2016
Revised: February 9, 2017
Published: February 13, 2017

DOI: 10.1021/acs.langmuir.6b04094
Langmuir 2017, 33, 4367−4385

hysteresis contact angles via the disjoining/conjoining pressure isotherm? It is possible, as shown in part 1.

In the next section, part 2, the equilibrium of liquid droplets on soft deformable substrates is considered. As we already mentioned above, surface forces (disjoining/conjoining pressure) play a role in the region close to the apparent three-phase contact line. We show in part 1 that the disjoining/conjoining pressure determines both equilibrium and hysteresis contact angles. Is it the same in the case of soft deformable surfaces? Obviously this is the case but more complicated than the case of solid nondeformable substrates. There are a very limited number of publications on the influence of the disjoining/conjoining pressure in this area in spite of considerable interest in the subject. We suggest a new way to calculate an equilibrium contact angle on a soft deformable surface based on the disjoining/conjoining pressure isotherm and a simple model of an elastic deformable solid. Note that in part 2 we calculate only the equilibrium contact angle, not hysteresis contact angles. The calculation of the hysteresis contact angles on soft solids based on the disjoining/conjoining pressure isotherm is to be undertaken in the future.

Now we turn to some applications of wetting and spreading. Blood is probably the most important liquid in our life. There is no need to explain how complex blood is. However, it turns out that from the hydrodynamic point of view blood is a relatively simple power low-shear-thinning non-Newtonian liquid (according to direct measurements of blood viscosity). On the basis of this fact, a theory is developed in part 3 to describe the spreading/imbibition behavior of blood droplets over thin porous substrates. The predicted theoretical dependencies are in reasonable agreement with the experimental data of the same process.

Trisiloxane surfactants, or superspreaders, are probably the most well known surfactants, which promote the fastest spreading over moderately hydrophobic substrates but still show only partial spreading over highly hydrophobic surfaces.[3] In spite of the wide applications of trisiloxanes, unfortunately they cannot be used in food, pharmaceutical, and other industries because of their special properties, which is why further investigations in the area related to superspreading are still in progress. The idea of the experimental research below is to investigate the new synergetic composition of surfactants that are capable of improving the wetting properties of aqueous formulations and providing fast spreading over hydrophobic substrates as well as to identify the parameters affecting the rate of spreading and possible mechanisms enabling the fast spreading of surfactant solutions over hydrophobic substrates. Some results in this area are presented in part 4.

Finally, in part 5 we present our recent results on the spreading of complex surfactant/polymer mixtures over hair tresses. The available investigations in this area focus on the interaction of a single hair fiber with different solutions. However, below the substrate is a bundle of hair where we observed the wetting transition of surfactant/polymer mixtures.

Contact Angle Hysteresis on Smooth Homogeneous Solid Surfaces via Disjoining/Conjoining Pressure. The phenomenon of contact angle hysteresis is usually attributed to the roughness and/or chemical heterogeneity of the surface. Although these properties of the substrate play a significant role in the contact angle hysteresis, they are not the sole reason for the hysteresis phenomenon. Convincing proof of the existence of contact angle hysteresis even on smooth homogeneous surfaces has been presented earlier.[4−7] The most obvious example observed experimentally is a hysteresis of the liquid meniscus in thin free liquid films[8−10] in which the hysteresis cannot be justified by the roughness and/or heterogeneity of the surface. It is demonstrated below that both static advancing and receding contact angles on smooth homogeneous solid surfaces can be found according to the disjoining/conjoining pressure isotherm. In spite of considerable interest in the hysteresis of the contact angle (over more than 100 years), it has not been found before.

Contact angle hysteresis for a liquid droplet on smooth, homogeneous solid surfaces was calculated earlier[1] according to the surface forces action and quasi-equilibrium phenomena. The developed theory was applied to the calculation of the contact angle hysteresis in a capillary meniscus and droplet.[11,12] On smooth homogeneous surfaces, contact angle hysteresis can be observed under partial wetting conditions only. In this case, a disjoining/conjoining pressure isotherm has an s-shaped form caused by the combined action of the following components:[2]

(1) The electrostatic component arising from the overlap of the electrical double layers

$$\Pi_E = RTc_0(\exp(\varphi) + \exp(-\varphi)) - 2RTc_0 - \frac{(RT)^2\varepsilon\varepsilon_0}{2F^2}\left(\frac{\partial\varphi}{\partial y}\right)^2 \quad (1)$$

where R is the universal gas constant, T is the temperature in K, F is Faraday's constant, ε and ε_0 are respectively the dielectric constants of water and vacuum, c_0 is the electrolyte concentration, y is the coordinate normal to the liquid−vapor interface, and φ is the dimensionless electric potential in units of F/RT.

The electric potential φ in eq 1 is related to the surface charge density σ as[2]

$$\sigma_h = \varepsilon\varepsilon_0\frac{RT}{F}\left(\frac{\partial\varphi}{\partial y}\right)_{y=h} \quad \text{for the liquid/vapor interface}$$

$$\sigma_s = -\varepsilon\varepsilon_0\frac{RT}{F}\left(\frac{\partial\varphi}{\partial y}\right)_{y=0} \quad \text{for the solid/liquid interface}$$

(2) The structural component is usually related to the interfacial layers as a result of water molecule dipole orientation.

This component is considered[13] as described by a two-term expression

$$\Pi_S = K_1\exp(-h/\lambda_1) + K_2\exp(-h/\lambda_2) \quad (2)$$

where K_1, K_2 and λ_1, λ_2 are the experimental constants corresponding to the magnitude and characteristic length of the short-range (1) and long-range (2) structural interactions, respectively.

(3) The van der Waals molecular component[2]

$$\Pi_M(h) = \frac{A}{6\pi h^3} \quad (3)$$

where $A = -A_H$ and A_H is the Hamaker constant. It should be noted that the van der Waals component effect is greatly exaggerated in most of the literature. $\Pi_M(h) \to \infty$ at $h \to 0$; however, the disjoining/conjoining pressure is a macroscopic value that is valid only at $h \gg$ molecular dimension. Under the latter condition and for aqueous solutions, other components of

DOI: 10.1021/acs.langmuir.6b04094
Langmuir 2017, 33, 4367−4385

the disjoining/conjoining pressure contribute equally or more than the van der Waals component.

The sum of the above-mentioned components leads to the following disjoining/conjoining pressure isotherm:[2,13]

$$\Pi(h) = \Pi_M(h) + \Pi_E(h) + \Pi_S(h) \quad (4)$$

Two possible disjoining/conjoining pressure isotherms are shown in Figure 1. Curves 1 and 2 correspond to the complete

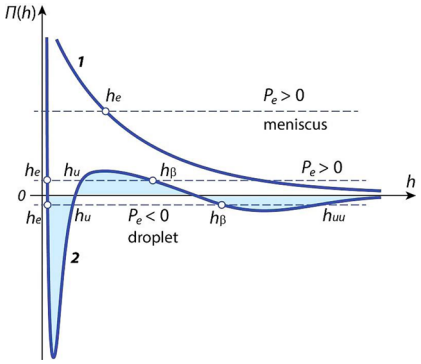

Figure 1. Schematic presentation of two possible disjoining/conjoining pressure isotherms: (1) complete wetting case and (2) partial wetting case. h_e, h_u, h_{uu}, and h_β are the thicknesses of stable, unstable, unstable, and metastable wetting films, respectively.[1,2]

wetting and the partial wetting cases, respectively. The hysteresis phenomenon occurs when three (in the case of the capillary meniscus) or four (in the case of droplets) intersections of a straight line of pressure P_e (Figure 1) with the disjoining/conjoining pressure isotherm are observed, which is possible only for the partial wetting case (isotherm 2 in Figure 1). The film thicknesses h_β corresponds to a metastable equilibrium thickness and h_u and h_{uu} correspond to unstable thicknesses; only h_e is related to a thermodynamically stable equilibrium thickness of the flat liquid film.[1,2]

The equilibrium condition of a two-dimensional droplet or capillary meniscus is described by the following equation (negligible influence of gravity):[1,2]

$$\frac{\gamma_{lv} h''}{(1 + h'^2)^{3/2}} + \Pi(h) = P_e \quad (5)$$

In the above equation, $h(x)$ is an equilibrium liquid profile and γ_{lv} is the liquid–vapor interfacial tension. All h, h', and h'' are functions of the x coordinate (Figure 2).

The excess pressure P_e in eq 5 is caused by a curvature of the liquid/vapor interface and is described by Kelvin's equation:[14]

$$P_e = \frac{RT}{v_m} \ln \frac{p_s}{p} = \pm \frac{\gamma_{lv}}{r_e} \quad (6)$$

Here, $P_e = P_v - P_l$, where P_l and P_v are the pressures in the liquid and vapor phases, respectively; v_m is the molar volume of liquid; and p_s and p are the saturated vapor pressure over a flat and curved surfaces, respectively. For a droplet, the excess pressure P_e is negative (pressure in the liquid exceeds the pressure in the vapor phase). According to eq 6, the condition $P_e < 0$ can take place only if $p > p_s$, hence droplets can exist at equilibrium with the oversaturated vapor only.

For a meniscus, the excess pressure is positive, $P_e > 0$, and on the basis of Kelvin's equation, $p < p_s$, the meniscus can be at equilibrium with undersaturated vapor. The equilibrium meniscus

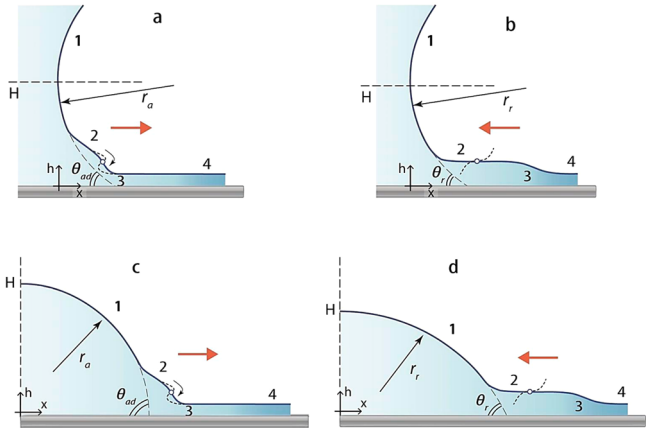

Figure 2. Transformation of the liquid profile of a capillary meniscus (a, b) and droplet (c, d) under conditions of advancing (a, c) and receding (b, d): (1) spherical meniscus or droplet; (2) transition region with a "critical" marked point (see explanation in the text), (3) flow region, and (4) flat film. A dashed line near the marked point indicates the transition profile just after the contact angle reaches the critical value θ_{ad}, the onset of the caterpillar motion. Adapted from ref 11. Copyright 2016 American Chemical Society.

can exist for both complete and partial wetting cases, whereas the equilibrium droplet spreads out in the case of complete wetting: it can exist only under partial wetting conditions.

When a pressure in the liquid grows, the interfacial profile of the droplet or meniscus compensates for the excess pressure at the expense of the curvature change, so the contact angle also grows. Under these conditions a macroscopic movement of the liquid profile is not observed but the profile moves microscopically. This process can continue over a long period of time if evaporation/condensation effects are negligible. At the moment when a critical value of the liquid pressure or contact angle θ_{ad} is achieved, the meniscus or droplet starts moving macroscopically. If the pressure under the liquid profile is decreased, then a similar phenomenon takes place: the profile does not recede until a critical pressure and the related critical contact angle, θ_r, are achieved. Therefore, in the range $\theta_r < \theta < \theta_a$, the profile is macroscopically immobile, and only microscopic movement occurs.

If the pressure in liquid is increased, the profile incline becomes steeper near the critical point[1] in the transition zone (Figure 2a,c). In the region of thin films, flow zone 3 exists where a viscous resistance is very high and the profile moves very slowly. Under a certain value of pressure, the liquid profile slope reaches a value of $\pi/2$ at the critical point; the flow expands gradually to a region of thick β films[1] and a fast "caterpillar motion" starts (Figure 2a,c).

If the pressure in liquid is decreased, then the slope of the liquid profile in the transition zone in a vicinity of a critical marked point (Figure 2b,d) becomes more flat. As in the previous case of advancing, the flow zone with high viscous resistance is observed in the region of thin films (Figure 2b,d) where the droplet or meniscus moves very slowly. When a critical value of the pressure is achieved, the discontinuous character of the profile should be expected near the critical marked point; however, this behavior of the profile is obviously impossible. As a result, the profile sliding over the thick β film is observed. The existence of a thick β film behind the receding meniscus was investigated experimentally for aqueous solutions in quartz capillaries.[13,15] This experimental fact agrees with conclusions

DOI: 10.1021/acs.langmuir.6b04094
Langmuir 2017, 33, 4367–4385

following from the theory of static contact angle hysteresis on smooth, homogeneous substrates.[1]

It has been assumed below that in the case of small deviations from equilibrium, eq 5 can be used in which P_e is substituted by a nonequilibrium pressure P (details in refs 1, 11, and 12). Below, a short description of the expressions applied for the contact angle calculations is presented.[11,12]

After the multiplication of eq 5 by h', integration with respect to x from 0 to x (Figure 2, $h = H$, $h' = \infty$ at $x = 0$ for a meniscus and $h = H$, $h' = 0$ at $x = 0$ for a droplet) gives

for a meniscus

$$\frac{1}{\sqrt{1 + h'^2}} = \frac{\psi(h, P)}{\gamma_{lv}} \tag{7}$$

where

$$\psi(h, P) = P(H - h) - \int_h^\infty \Pi(h)\, dh \tag{8}$$

for a droplet

$$\frac{1}{\sqrt{1 + h'^2}} = \frac{\gamma - \psi(h, P)}{\gamma_{lv}} \tag{9}$$

where

$$\psi(h, P) = -P(H - h) + \int_h^\infty \Pi(h)\, dh \tag{10}$$

where P is the nonequilibrium pressure corresponding to nonequilibrium conditions of the hysteresis transition (in contrast to the equilibrium pressure P_e).

The left-hand side of eqs 7 and 9 ranges in between 0 (at $h'^2 = \infty$) and 1 (at $h'^2 = 0$). Therefore, the right-hand side of eqs 7 and 9 should be at the same range. The latter determines the region where a solution of eqs 7 and 9 exists:

$$0 \le \psi(h, P) \le \gamma_{lv} \tag{11}$$

The extrema of $\psi(h, P)$ are obtained from $P = \Pi(h)$, like the equilibrium condition, i.e., from the intersection of the straight line P = const with the disjoining/conjoining pressure isotherm. For the equilibrium profile when $P = P_e$, the function $\psi(h, P_e)$ has an extremum and vanishes at $h = h_e$. The other extrema points correspond to the boundaries of the interval (11), i.e., to the values $\psi = 0$ and $\psi = \gamma_{lv}$ at points $h = h_1$ and $h = h_2$. The violation of one of the inequalities in (11) indicates the static advancing contact angle, θ_{ad}, and the violation of another condition determines the static receding contact angle, θ_r.

The expressions obtained for the cases of the capillary meniscus and droplet are shown in the Table 1.

The expressions for cos θ_i have been obtained using the relation $P_i = \gamma_{lv}(\cos\theta_i - 1)/H_i$ for a droplet and $P_i = \gamma_{lv}\cos\theta_i/H_i$ for a meniscus (here i = ad, e, r). The expression for equilibrium contact angle θ_e in Table 1 agrees with the known Frumkin equation in terms of disjoining/conjoining pressure.[2,16] The expressions for cos θ_i in Table 1 have similar forms for the cases of meniscus and droplet; however, the numerical values of the contact angle θ_i calculated by these expressions differ because the values h_1, h_2, and h_e are different for the meniscus and droplet.

The disjoining/conjoining pressure isotherm used in calculations of the contact angles hysteresis was computed earlier[11,12] and corresponds approximately (as much as possible) to the case of aqueous droplets in contact with a glass surface.[17] The isotherm parameters for both cases are the same:[12]

Table 1. Calculations of Hysteresis Contact Angles

	meniscus	droplet
values of $\psi(h, P)$ function	advancing state $\psi(h_1, P_a) = 0$; receding state $\psi(h_2, P_r) = \gamma_{lv}$	advancing state $\psi(h_1, P_a) = \gamma_{lv}$; receding state $\psi(h_2, P_r) = 0$
advancing angle	$\cos\theta_{ad} = \frac{\Pi(h_1)h_1}{\gamma_{lv}} + \frac{1}{\gamma_{lv}}\int_{h_1}^\infty \Pi\, dh$	
equilibrium angle	$\cos\theta_e = 1 + \frac{\Pi(h_e)h_e}{\gamma_{lv}} + \frac{1}{\gamma_{lv}}\int_{h_e}^\infty \Pi\, dh$	
receding angle	$\cos\theta_r = 1 + \frac{\Pi(h_2)h_2}{\gamma_{lv}} + \frac{1}{\gamma_{lv}}\int_{h_2}^\infty \Pi\, dh$	

$\sigma_s = -150$ mC, $\sigma_h = 120$ mC, $c_0 = 1 \times 10^{-2}$ mol/m^3, $A = 3.5 \times 10^{-20}$ J, $K_1 = 2.0 \times 10^7$ Pa, $K_2 = -1 \times 10^4$ Pa, $\lambda_1 = 3.6 \times 10^{-9}$ m, and $\lambda_2 = 26 \times 10^{-9}$ m. The surface tension $\gamma_{lv} = 72.7 \times 10^{-3}$ N/m corresponding to a dilute aqueous NaCl solution was assumed.

The calculation of contact angles θ_{ad}, θ_r and θ_e was made at different capillary widths H and the droplet volumes V_a. The calculated results are presented in Figure 3 and show that $\theta_r < \theta_e < \theta_{ad}$, as expected. The calculated values of advancing contact angle ~57° and receding contact angle ~9° correspond to available experimental data.[1,17]

Figure 3a,b demonstrates that contact angles for droplets and menisci depend on droplet/capillary size in different ways: the contact angles for meniscus increase with capillary size, but for the droplet, oppositely, the larger the droplet, the smaller the contact angle. The experimental data in similar systems[18] confirm this dependency in capillaries (Figure 3a).

Figure 3a demonstrates an interesting peculiarity for the dependence of the receding contact angle, θ_r: while the capillary width is decreased, the transition from partial to complete wetting is observed (θ_r becomes equal to zero) at a capillary size of $H \approx 3 \times 10^{-6}$ m. This type of transition for the contact angles in thin capillaries was discussed earlier.[19]

Figure 3a,b shows that the equilibrium contact angle remains almost constant with the capillary/droplet size. This angle just slightly varies in the case of very thin capillaries and becomes equal to about 10° for both the capillary and droplet cases. Figure 3 shows also that for both cases the equilibrium angles are closer to the receding values than to the advancing ones, i.e., $\theta_e - \theta_r \ll \theta_{ad} - \theta_e$. This fact differs from the well-adopted opinion that the equilibrium contact angle value can be reliably approximated by the value of the static advancing contact angle. The obtained data demonstrate that for both droplets and capillaries (Figure 3a,b) the values of the equilibrium contact angles are closer to the receding angle values.

The character of the predicted dependency of the contact angle on the droplet volume has experimental confirmation.[20,21] The phenomenon of thick β-films formation behind the receding meniscus was experimentally investigated in capillaries by Churaev's group.[13,15] The formation of the β films behind the receding droplet requires the further experimental confirmation.

Equilibrium of Droplets on a Deformable Substrate: Influence of Disjoining/Conjoining Pressure. The equilibrium of a liquid droplet on a solid substrate is frequently depicted on the basis of Young's equation.[22] This simplified equation involves the balance of the horizontal forces, leaving the vertical force unbalanced. The latter is possible in the case of a rigid substrate but should be reconsidered in the case of deformable substrates. It was shown earlier[1] that disjoining/conjoining

DOI: 10.1021/acs.langmuir.6b04094
Langmuir 2017, 33, 4367−4385

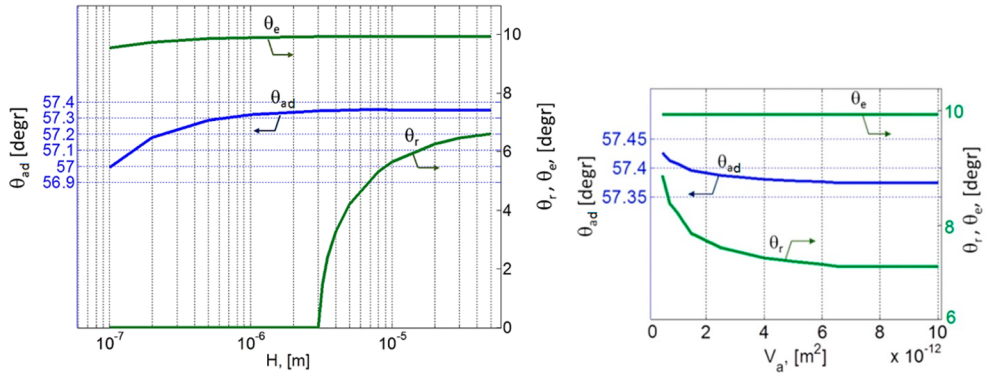

Figure 3. Effect of the capillary width (a) and the droplet volume (b) on the contact angles values calculated by equations from Table 1.[11,12] The volume of the flat (two-dimensional) droplet is expressed in m^2. Two vertical axes are used in the plots; arrows on the curves show the direction to the appropriate axis.

pressure action in the vicinity of the apparent three-phase contact line results in a deformation of a deformable solid substrate.

Note that direct application of Young's equation leads to a deformation singularity at the three-phase contact line, i.e., the substrate deformation goes to infinity:[23−27] these investigation showed that all equilibrium properties (i.e., contact angle, droplet radius, etc.) of the system under consideration rely upon the selected artificial length parameter that determines the width of the zone near the contact line where surface tension is applied. It is shown below that disjoining/conjoining pressure, which is a real physical phenomenon, determines the deformation of soft surfaces. It is shown in part 1 that the shape of the disjoining/conjoining pressure isotherm determines the shape and the contact angle of the droplet at equilibrium[1] and even hysteresis static advancing and receding contact angles on solid rigid substrates. It is shown below that the combined action of disjoining/conjoining pressure and the elasticity of the deformable substrate determines an apparent contact angle on deformable substrates.

The problem of the equilibrium of the droplet on a deformable substrate has recently attracted a lot of interest, and a number of experimental studies (e.g., refs 28−30) have recently been published on the investigation of the deformation of soft substrates by liquid droplets near the apparent contact line. The first attempt to consider the disjoining/conjoining pressure action in the vicinity of the three-phase contact line in the case of deformable substrates was undertaken in ref 31, which was followed by other publications.[32,33] In ref 34, a simplified mathematical model is presented that incorporates the effects of both capillary and disjoining/conjoining pressure on the substrate deformation.

A simple Winkler model of solid deformation is used below. According to the Winkler model, there is a linear relationship between the local deformation and the applied local stress.[35,36]

The deformation of the deformable substrate is local, and it is directly proportional to the applied pressure, P. According to the Winkler model

$$h_s = -KP \tag{12}$$

where K is the elasticity coefficient and h_s is the local deformation of the substrate due to the presence of the applied pressure, P, from the droplet above (Figure 4).

Let P_v be the pressure in the ambient vapor. Under the action of the pressure from the ambient vapor, the solid deformation is

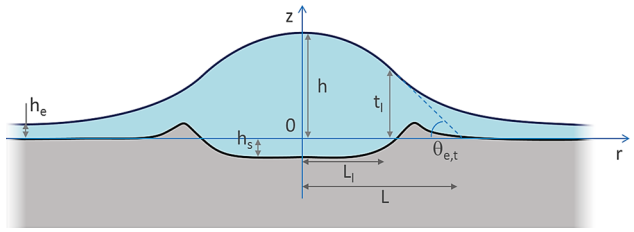

Figure 4. Schematic diagram of an equilibrium liquid droplet on a deformable substrate. The macroscopic contact angle is determined as an intersection of the continuation of the spherical part with the plane of the initial deformable substrate. All notations are given directly in the text.

$$h_{se} = -KP_v \tag{13}$$

The deformed solid substrate is covered by an equilibrium liquid thin film, which is calculated according to the combination of the well-known Kelvin equation and the disjoining/conjoining pressure isotherm[1]

$$\Pi(h_e) = P_e = \frac{RT}{\nu_m} \ln \frac{p_s}{p} \tag{14}$$

where ν_m is the molar volume of the liquid, T is the temperature in K, R is the gas constant, and p is the vapor pressure, which is higher than the saturated pressure p_s. We remind the reader that a droplet can be at equilibrium with oversaturated vapor only according to Kelvin's equation.

The excess free energy of the equilibrium thin film on the deformed solid per unit area is given by

$$\frac{\Phi_{e,film}}{S_{film}} = \gamma_{lv} + \gamma_{sl} + P_e h_e + \frac{h_{se}^2}{2K} + \int_{h_e}^{\infty} \Pi(h)\, dh \tag{15}$$

where $P_e = P_v - P_l$ and γ_{lv} and γ_{sl} are the liquid−vapor and solid−liquid interfacial tensions, respectively. This free energy should be subtracted from the free energy of the droplet on the deformable substrate; otherwise, the excess free energy of the droplet is infinite. Hence, the excess free energy of the droplet on a deformable solid substrate is as follows (Figure 4)

$$\phi - \phi_{e,film} = \gamma_{lv}\Delta S + \gamma_{sl}\Delta S_s + \Delta V + F_{surface\ forces} + F_{deformation} \tag{16}$$

DOI: 10.1021/acs.langmuir.6b04094
Langmuir 2017, 33, 4367−4385

where Δ means "as compared to a flat equilibrium film".

Equation 16 can be rewritten as

$$\Phi - \Phi_{e,film} = 2\pi \int_0^\infty f(h, h', h_s, h'_s)\, dr \tag{17}$$

where

$$f(h, h', h_s, h'_s) = r\left[\begin{array}{c} \gamma_{lv}\sqrt{1 + h'^2(r)} - \gamma_{lv} + \gamma_{sl}\sqrt{1 + h_s'^2(r)} - \gamma_{sl} + \\ P_e(h - h_s) - P_e h_e + \frac{h_s^2}{2K} - \frac{h_{se}^2}{2K} \\ + \int_{h-h_s}^\infty \Pi(h)\, dh - \int_{h_e}^\infty \Pi(h)\, dh \end{array}\right] \tag{18}$$

In above equations, r is the radial coordinate and γ_{sl} is the solid−liquid interfacial tension. The expression under the integral in eq 17 tends to zero as the radius, r, tends to infinity.

Under equilibrium conditions, the excess free energy (eq 17) should decrease to its minimum value. To satisfy this condition, the first variation of excess free energy (eq 17) should be zero, which results in two Euler equations for the droplet and deformable substrate profiles:[34]

$$\frac{\gamma_{lv}}{r}\frac{d}{dr}\frac{rh'}{(1 + h'^2)^{1/2}} + \Pi(h - h_s) = P_e \tag{19}$$

$$\frac{\gamma_{sl}}{r}\frac{d}{dr}\frac{rh'_s}{(1 + h'^2_s)^{1/2}} - \Pi(h - h_s) - \frac{h_s}{K} = -P_e \tag{20}$$

Equations 19 and 20 are a system of two interconnected differential equations for two unknown profiles: the liquid droplet, $h(r)$, and the deformed solid substrate, $h_s(r)$. When the case of a low slope approximation is used,[34] $h'^2 \ll 1$, $h_s'^2 \ll 1$, which is valid at small contact angles. Note that eq 19 is different from the usual equation for the droplet on a rigid substrate because now the disjoining/conjoining pressure term depends on the profile of the deformable substrate, $h_s(r)$, which is determined according to eq 20. Equations 19 and 20 are coupled and can be solved numerically only in the case of a low slope approximation, which is the reason that below the problem has been simplified further to obtain an analytical solution. For this purpose, a simple disjoining/conjoining pressure isotherm (linear function of h (Figure 5)) was adopted[34]

$$\Pi(h) = \begin{cases} P_1 - ah \text{ at } h \le t_1 \\ 0 \text{ at } h > t_1 \end{cases} \tag{21}$$

where P_1, P_2, and t_o are defined in Figure 5 and t_1 is the range of surface forces action.

The selected linear disjoining/conjoining pressure isotherm $\Pi(h)$, according to eq 21, was successfully used earlier in refs 1 and 37 and still captures the essential properties of the disjoining/conjoining pressure isotherm in spite of considerable simplification: (i) it satisfies the stability condition, $\Pi'(h) < 0$ when $h < t_1$; (ii) the influence of surface forces is short-ranged and the radius of their action is defined by t_1; and (iii) it relates to the partial wetting case for the proper choice of the disjoining/conjoining pressure parameters (Table 2).

Disjoining/conjoining pressure takes action in the three-phase contact line region. Therefore, substrate deformation near the contact line depends largely upon the parameters of the disjoining/conjoining pressure isotherm.

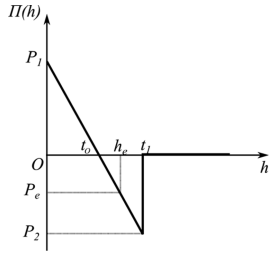

Figure 5. Simplified disjoining/conjoining pressure isotherm adopted below for calculations.

Table 2. Parameters Selected for the Calculation of the Droplet Profile and Substrate Deformation

physical property	value
γ_{lv}	72 dyn/cm
t_1	3×10^{-6}cm
t_0	7×10^{-7}cm
a	1×10^{-11}dyn/cm^3
K	1×10^{-11} cm^3/dyn
P_e	-1×10^5 dyn/cm^2
γ_{sl}	10 dyn/cm

Results of calculations according to eqs 19 and 20 for both the droplet and substrate profiles are presented for one special case in Figure 6.

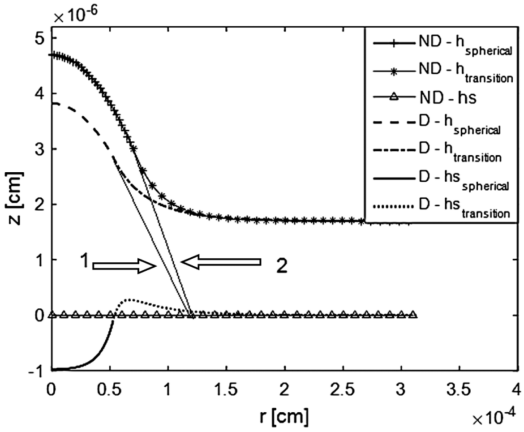

Figure 6. Comparison between the profiles of the droplet and substrate for a nondeformable (ND) and deformable (D) substrate. The contact angle on a deformable substrate, 1, is lower than that on a nondeformable substrate, 2.

The calculations provided in ref 34 proved that the apparent equilibrium contact angle that a droplet makes with the substrate is lower on a deformable substrate as compared to the corresponding contact angle on a nondeformable substrate. It is shown also that there are three substantially different length scales that determine the extension of the deformed region inside the soft solid under the droplet.[34] This conclusion shows that the deformation of the solid is a more complex phenomenon than usually assumed (only one length scale).

Kinetics of Wetting and Spreading of Non-Newtonian Liquid over Porous Substrates. The wetting and spreading of pure Newtonian liquids over solid surfaces has been well documented in the literature from both theoretical and experimental points of view.[1] However, most commonly found liquids in our everyday life such as blood, shampoos, hair colorants, and paints

DOI: 10.1021/acs.langmuir.6b04094
Langmuir 2017, 33, 4367−4385

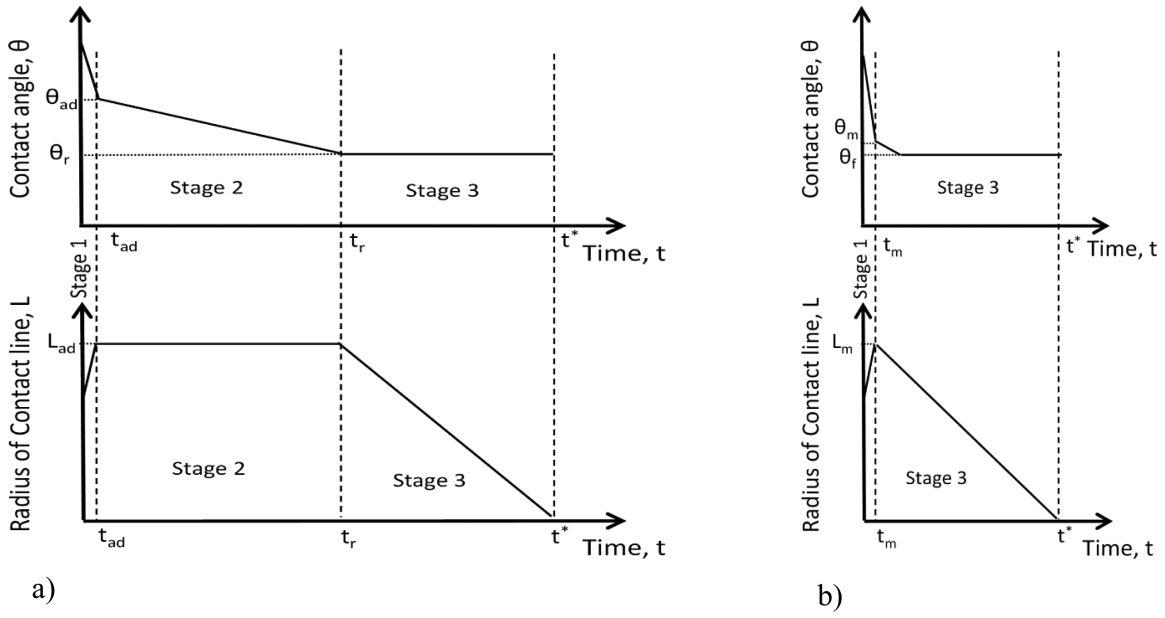

Figure 7. Spreading/imbibition of a droplet over a porous surface: (a) partial wetting case: three stages. L_{ad} is the maximum radius of the droplet base, θ_{ad} is the advancing contact angle, t_{ad} is the time when θ_{ad} is reached, θ_r is the receding contact angle, t_r is the time when θ_r is reached, and t^* is the time of droplet disappearance. (b) Complete wetting case: there are two stages. L_m is the maximum value of the droplet base radius, t_m is the time when L_m is reached, θ_m is the contact angle at t_m, t^* is the time of droplet disappearance, and θ_f is the final contact angle at t^*. Note that stage 2 is absent in the complete wetting case. Reproduced with permission from ref 54. Copyright 2015 Elsevier B.V.

are colloidal suspensions or polymeric solutions that exhibit non-Newtonian behavior. Frequently, the surfaces where these solutions are applied, such as skin, hair tresses, and textile materials, are porous. The wetting and spreading of non-Newtonian liquid droplets over smooth homogeneous substrates have been theoretically investigated in the literature using both hydrodynamic[38−43] and molecular kinetic theory models.[44] Nonetheless, wetting and spreading conditions of a droplet over a porous surface are clearly different because of the existence of a porous layer. This system has been explored in the case of Newtonian liquid droptes.[45−47]

The wetting and spreading of biological fluids have been less widely studied in spite of the potential applications in medical science. Brutin et al.[48−51] investigated the wetting, spreading, and evaporation dynamics of blood droplets, which exhibit shear-thinning non-Newtonian behavior, over solid surfaces. They found a spreading law of $L \approx t^{0.65}$ in the initial stages of spreading in which the process is controlled by a competition between viscous and surface tension forces whereas at later stages of spreading the spreading exponent ($L \approx t^{0.19}$) was higher than that in Tanner's law (i.e., $L \approx t^{0.1}$) because of the effect of Marangoni stresses and humidity. Below we present our most recent theoretical and experimental findings on the wetting/imbibition of blood droplets over dry, thin porous substrates.[52−54] This process is a representation of dried blood spot sampling, which is a technique for blood collection.[55] In this technique, a thin porous surface such as cotton fibers, cellulous fibers, and polymer membranes is used to collect a small blood droplet: the droplet spreads over a porous substrate, where it imbibes into the substrate and is preserved as a dried spotted sample. A hydrodynamically based mathematical model under lubrication approximation theory has been developed to describe the dynamics of wetting/imbibition of blood droplets in the case of partial and complete wetting over thin porous layer.[53,54]

The spreading/imbibition process of a droplet over a porous surface can be subdivided into three subsequent stages in a partial wetting case (Figure 7a):[54] stage (1), fast spreading of the droplet until its base radius expands and the contact angle decreases to the static advancing contact angle; stage (2), constant radius of the contact line (at its maximum value) while the contact angle decreases from the value of a static advancing to static receding contact angle; stage (3), a shrinkage of the droplet base at the fixed static receding contact angle until complete disappearance. The main characteristic of partial wetting is the contact angle hysteresis: this results in the existence of stage 2, when the droplet edge is pinned. However, there is no hysteresis in complete wetting; therefore, stage 2 in partial wetting is absent in complete wetting behavior (Figure 7b), and there are only two stages of spreading.[52,53]

Blood with different hematocrit levels was prepared, and droplets with a known volume were deposited on different porous substrates: commercial untreated Whatman 903 filter paper, silanized Whatman 903 filter paper, and nitrocellulose membranes with pore sizes of 0.2 and 8 μm. The details of the experimental procedure can be found in refs 52 and 54. It was shown that the rheological model of blood with different hematocrit levels can be fitted by the well-known Otswald−de Waele power law relationship, $\eta = k\dot{\gamma}^{n-1}$, with different k and n values, where k is flow consistency index, n is the flow behavior index, and $\dot{\gamma}$ is the shear rate.

Figure 8 shows the schematic of axisymmetric droplet spreading on a porous surface with a thickness of Δ, which was considered to be much smaller than the droplet height, i.e., $\Delta \ll h^*$, where h^* is the scale of the droplet height. It was assumed that the slope of the droplet profile is low, $h^*/L^* \ll 1$, where L^* is the scale of the drop base. Only small droplets are under consideration; that is, the action of gravity was neglected. Therefore, the droplet profile in the case of capillary spreading, except for a small region close to the three-phase contact line, remains a spherical cap. The time evolution of the spreading radius, $L(t)$, the droplet height, $h(r, t)$, and the radius of the

DOI: 10.1021/acs.langmuir.6b04094
Langmuir 2017, 33, 4367−4385

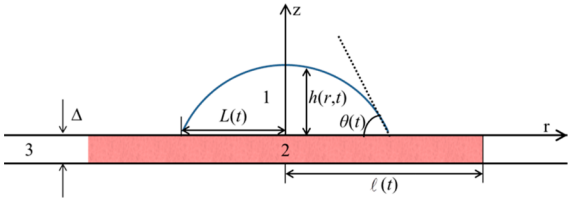

Figure 8. Schematic of axisymmetric droplet spreading on a porous surface. (1) Liquid drop, (2) wetted area in the porous layer, and (3) dry area in the porous layer. $L(t)$ is the radius of the droplet base, $l(t)$ is the radius of the wetted area, $\theta(t)$ is the contact angle, and Δ is the thickness of the porous surface. Reproduced with permission from ref 53. Copyright 2015 Elsevier B.V.

wetted area inside the porous substrate, $l(t)$, were monitored during the spreading experiments.

Complete Wetting. The drop motion in the case of complete wetting was perceived to be a superposition of two motions:[47,53] (a) an expansion of the drop base as a result of spreading over an already saturated part of the porous layer and (b) a shrinkage of the drop base as a result of the imbibition into the porous substrate. Accordingly, the following equation can account for the rate of the drop base motion

$$\frac{dL}{dt} = v_+ - v_- \tag{22}$$

where v_+ and v_- are the expansion and the shrinkage velocities, respectively.

Considering the previous assumption, the following system of differential equations was deduced in ref 53 for the time evolution of the radius of both the droplet base, $L(t)$, and the wetted radius of the porous substrate, $l(t)$, in the case of complete wetting

$$\frac{dL}{dt} = \frac{\alpha_n \left(\frac{V}{V_0}\right)^{1/3} \left(\frac{n}{2n+1}\frac{\lambda}{\alpha_n}\left(\frac{\gamma_{lv}}{k}\right)^{1/n}\frac{V_0^{(n+2)/n}}{(2\pi)^{(n+2)/n}}\right)^{\alpha_n}}{(t+t_0)^{1-\alpha_n}} - \frac{2L\pi m\Delta}{3}\frac{K_n}{V_0 - \pi m\Delta l^2}$$
$$\left[\frac{(1-n)p_c}{k(l^{1-n} - L^{1-n})}\right]^{1/n} \tag{23}$$

$$\frac{dl}{dt} = \frac{K_n}{l}\left[\frac{(1-n)p_c}{k(l^{1-n} - L^{1-n})}\right]^{1/n} \tag{24}$$

where γ_{lv} is the surface tension of blood; V and V_0 are the volume and initial volume of the drop, respectively; t_0 is the duration of the initial fast stage of spreading that is close to zero; and $\alpha_n = \frac{n}{3n+7}$. As was mentioned above, n is the flow behavior index of the power law viscosity; λ is a constant, determined in ref 1; m and K_n are the porosity and permeability of the porous layer, respectively; and p_c is the capillary pressure inside the pores of the porous layer. These equations were made dimensionless using the following scales: $\overline{L} = L(t)/L_m$, $\overline{l} = l(t)/l^*$, $\overline{\theta} = \theta(t)/\theta_m$, and $\overline{t} = t/t^*$. L_m is the maximum radius of the droplet base that is reached at t_m, l^* is the final radius of the wetted area at the end of the process, θ_m is the contact angle at the maximum spreading radius, and t^* is the time of droplet disappearance. After that, the dimensionless equations were solved using initial and some additional conditions specified in ref 53 for blood samples with different hematocrit levels. Details of the mathematical model and calculations can be found in ref 53.

The results of experiments in refs 52 and 54 indicated that the blood droplet spreading/imbibition on both untreated and treated Whatman 903 filter papers was completely wetting. Although the silanization of filter paper resulted in a substantial increase in the dynamic contact angle, the process remained completely wetting. Figures 9−11 compare the experimental data with the predicted results for complete wetting cases. According to the figures, it is clear that all of the data indicate corresponding universal values with dimensionless parameters L/L_m, l/l^*, t/t^*, and θ/θ_m. The predicted results for blood droplets with different values of n are in good agreement with the experimental data. Nevertheless, the main conclusion is that both experimental data and the calculated results indicate noticeable universal behavior independent of n in dimensionless coordinates. As can be seen in Figures 9−11, only two stages of spreading have been identified in the case of complete wetting: a relatively fast initial stage of spreading followed by a shrinkage of the droplet base as a result of the droplet volume loss due to the imbibition into a porous substrate.

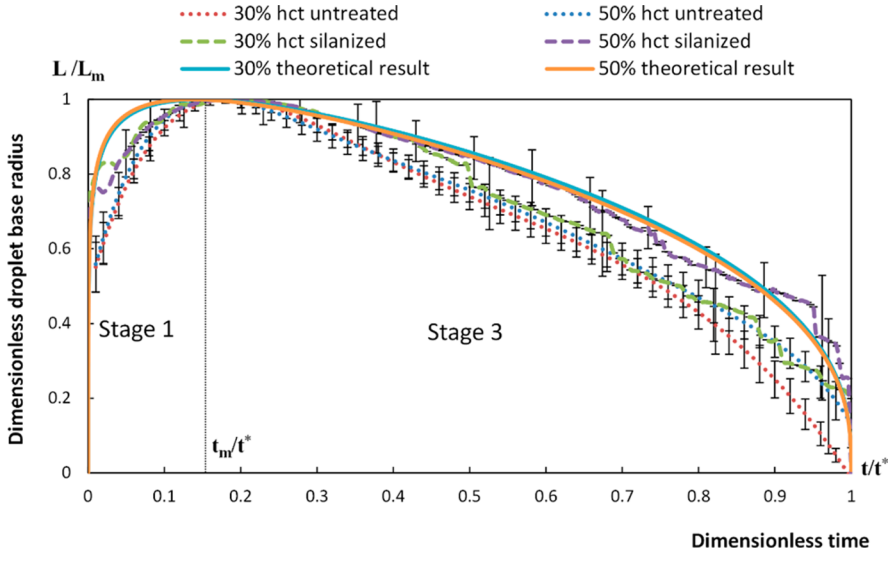

Figure 9. Dimensionless time evolution of the droplet base radius over silanized and untreated Whatman 903 paper. Adapted with permission from ref 54. Copyright 2015 Elsevier B.V.

DOI: 10.1021/acs.langmuir.6b04094
Langmuir 2017, 33, 4367−4385

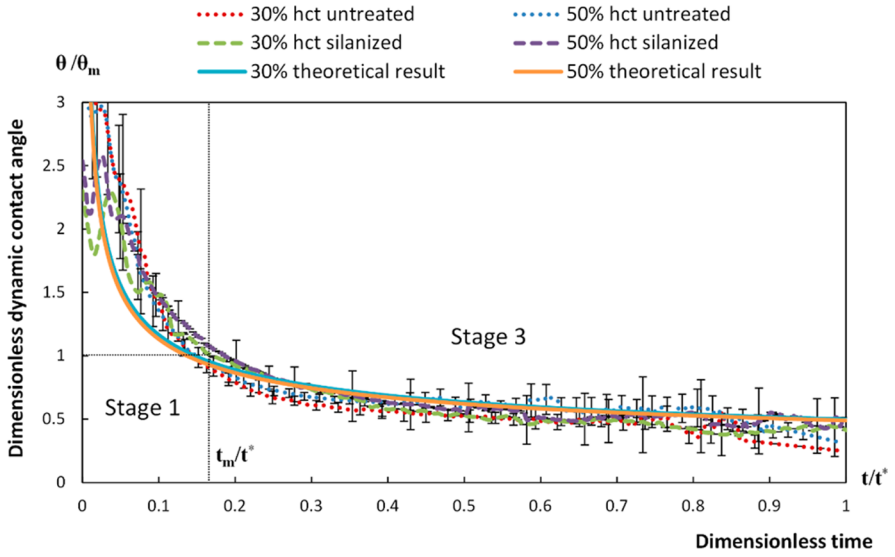

Figure 10. Dimensionless time evolution of the contact angle for blood spreading over silanized and untreated Whatman 903 paper. Adapted with permission from ref 54. Copyright 2015 Elsevier B.V.

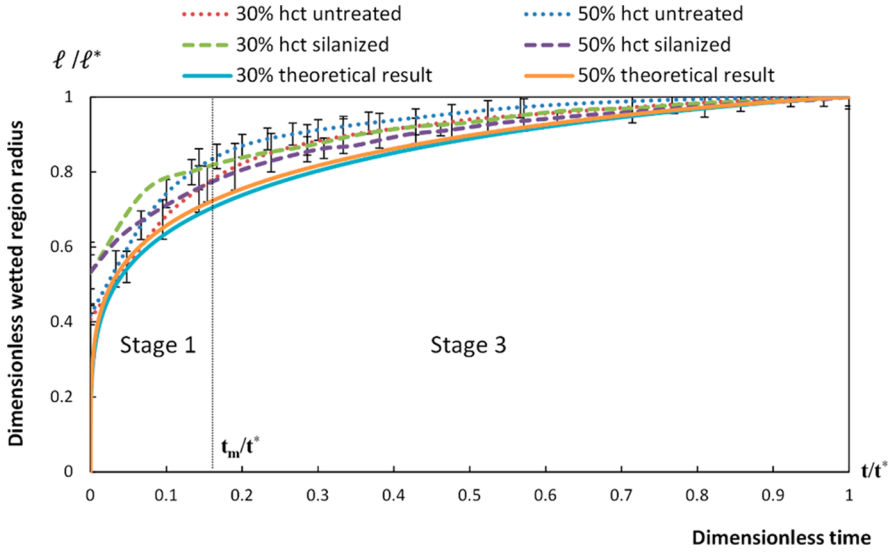

Figure 11. Dimensionless time evolution of the wetted radius inside the filter paper for blood spreading over silanized and untreated Whatman 903 paper. Adapted with permission from ref 54. Copyright 2015 Elsevier B.V.

Partial Wetting. According to ref 54, the blood droplets' spreading/imbibition on nitrocellulose membranes exhibits partial wetting behavior. The following dimensionless values were utilized to compare the behavior of blood spreading on different nitrocellulose membranes: $\overline{L} = L(t)/L_{ad}$, $\overline{l} = l(t)/l^*$, $\overline{\theta} = \theta(t)/\theta_{ad}$, and $\overline{t} = t/t^*$, where L_{ad} is the maximum droplet base radius, l^* is the final radius of wetted area, θ_{ad} is the advancing contact angle, and t^* is the final time of imbibition. In Figures 12−14, the time evolution of the dimensionless droplet base radius, contact angle, and the wetted radius is presented for partial wetting behavior. A corresponding universal behavior independent of bloods with different hematocrit level and n values is also clear here for different nitrocellulose membranes. The whole spreading process on nitrocellulose membranes can be subdivided into three stages, as shown earlier in Figure 7a, which is the main characteristic of the partial wetting behavior. However, note that the red blood cells did not penetrate nitrocellulose membranes of 0.2 μm pore size and only plasma could penetrate them. That is, the droplet base did not disappear at the end of process (Figure 12), and only stages 1 and 2 exist in

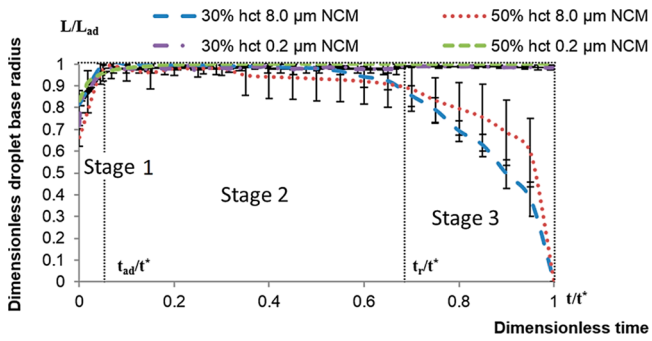

Figure 12. Dimensionless time evolution of the droplet base radius over a nitrocellulose membrane. In the case of a 0.2 μm nitrocellulose membrane (NCM), only stages 1 and 2 exist. Reproduced with permission from ref 54. Copyright 2015 Elsevier B.V.

DOI: 10.1021/acs.langmuir.6b04094
Langmuir 2017, 33, 4367−4385

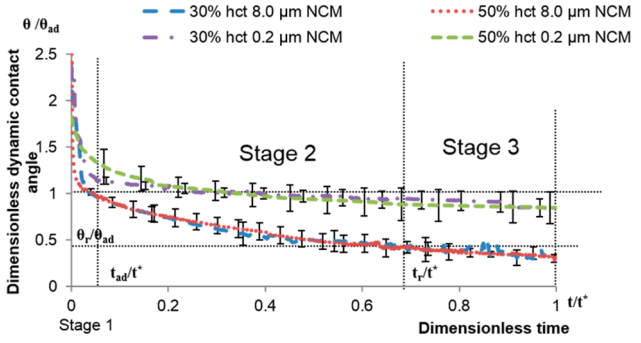

Figure 13. Dimensionless time evolution of the contact angle for blood spreading over nitrocellulose membrane. Note that in the case of a 0.2 μm nitrocellulose membrane (NCM), stage 3 is just a continuation of stage 2. Reproduced with permission from ref 54. Copyright 2015 Elsevier B.V.

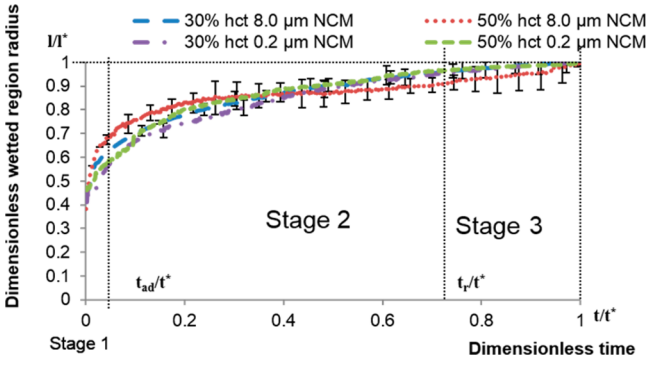

Figure 14. Dimensionless time evolution of the wetted radius inside the filter paper for blood spreading over nitrocellulose membrane. Note that in the case of a 0.2 μm nitrocellulose membrane (NCM), stage 3 is just a continuation of stage 2. Reproduced with permission from ref 54. Copyright 2015 Elsevier B.V.

this case. This observation suggests a completely new possibility to (i) investigate red blood cells and plasma separately and (ii) apply this technique to the nondestructive separation of living cells from aqueous solutions.

Kinetics of Spreading of Surfactant Solutions. A considerable number of artificial surfaces (mostly polymeric surfaces) and most natural surfaces (human/animal skin, leaves, grass, and so on) are hydrophobic, that is, not wet by water. However, the wetting of these surfaces by water is important and in many cases vital (agriculture, for example). How is water forced to spread over hydrophobic surfaces? The answer is to add surfactants to water. The best-known promoters of spreading over hydrophobic surfaces are trisiloxanes and their derivatives, which are referred to as superspreaders. In spite of considerable interest in the superspreading phenomenon in the literature, the nature of this phenomenon is yet to be understood. All attempts to understand the phenomenon directly have not resulted in a breakthrough. This is the reason that we decided to try a completely different approach: based on an investigation of surfactant mixtures, we would like to try to understand the nature of the phenomenon and to attempt to find a suitable substitute for trisiloxanes. The presence of surfactants promotes enhanced spreading of aqueous solutions over hydrophobic substrates. However, the addition of surfactant complicates the spreading process enormously even if the solution remains a Newtonian liquid with a constant viscosity independent of the shear rate. The complexity is caused by the dynamic nature of the surface tension of surfactant solutions: the surface tension of a pure liquid remains constant under isothermal conditions, whereas that of a surfactant solution depends on the surface age and can change upon surface deformation in the course of the spreading process.

When a new interface is forming, the interfacial tension is initially equal to that of the pure solvent (water for aqueous solutions), and then it decreases gradually due to both surfactant adsorption and/or transfer caused by Marangoni flow (for the liquid/fluid interface). Therefore, the spreading coefficient $\xi = \gamma_{sv} - (\gamma_{sl} + \gamma_{lv})$, where γ_{sv}, γ_{sl}, and γ_{lv} are the solid/vapor, solid/liquid, and liquid/vapor interfacial tensions, respectively, increases with time as a result of the decreases in γ_{sl} and γ_{lv} (and possible increase in γ_{sv}[1]) until the equilibrium values of solid/liquid and liquid/vapor interfacial tensions are reached. The dynamic surface tension on the leading edge of spreading (close to the three-phase contact line) can be higher than the equilibrium value that is caused by the expansion of a surface in the course of spreading. This could result in a smaller spreading coefficient and slower spreading. On the other hand, the difference in the surface tension between the region close to the three-phase contact line and the central part of the deposited drop can cause surface stresses, resulting in Marangoni flow in the direction of spreading, accelerating the spreading process. As a result of these and other factors, the kinetics of spreading of surfactant solutions is different from that of pure liquids. According to refs 56−58 in the case of the superspreading of aqueous surfactant solutions over hydrophobic surfaces, the droplets spread faster than do completely wetting liquids over hydrophilic surfaces (for example, oil over a glass surface). In the case of superspreading, the spread radius, L, is proportional to the square root of time, t, whereas in the case of complete wetting over hydrophilic surfaces, $L \approx t^{0.1}$. That is, the spreading exponent, α, characterizing the rate of spreading $L \approx t^{\alpha}$ is equal to 0.1 for completely wetting liquids on hydrophilic substrates and 0.5 for the case of superspreading over hydrophobic substrates.

The fastest spreading (superspreading) of highly hydrophobic substrates such as polyethylene and polypropylene is achieved using trisiloxane surfactants, referred to as superspeaders.[59−64] The equilibrium surface tension of trisiloxane solutions is rather low; however, it is not the sole reason for the superspreading behavior: the wetting properties of the trisiloxane surfactants are superior in comparison to those of fluorosurfactants despite the lower values of the equilibrium surface tension exhibited by fluorosurfactants.[65] One of the reason for that could be the better adsorption of trisiloxane surfactants on hydrocarbon solid substrates and therefore lower solid/liquid interfacial tension.[65]

The equilibrium surface tension of a surfactant solution levels off when the critical micelle concentration (CMC) or, in more general terms, the critical aggregation concentration (CAC) is reached. However, superspreading behavior starts at the critical wetting concentration (CWC), which often is higher than the CAC: CWC ≥ CAC.[66] The latter points out the importance of dynamic effects in the mechanism of superspreading and surfactant-enhanced spreading. It is noticeable that CWC does not depend on the substrate used for spreading.[66] Note that in the case of a very hydrophobic substrate, Teflon, only partial wetting has been detected at concentrations even above the CWC, which was the reason that the CWC was defined as the concentration above which the contact angle of surfactant solution on the substrate remains constant.

The mechanism of a fast spreading of surfactant solutions on hydrophobic surfaces (superspreading) is to be understood.

DOI: 10.1021/acs.langmuir.6b04094
Langmuir 2017, 33, 4367−4385

Promising hypotheses are as follows: (i) caterpillar motion at the three-phase contact line decreasing viscous energy dissipation;[1,67,68] (ii) Marangoni flow due to surfactant depletion near the three-phase contact line;[68−71] and (iii) a direct transfer of surfactant molecules in front of the moving three-phase contact line (autophilic phenomenon).[1] This phenomenon was directly experimentally confirmed in ref 72: (iv) the formation of bilayer self-assembled structures on the leading edge of spreading.[73,74] In ref 75, the available experiments on surfactant-enhanced spreading were reviewed, and its possible mechanisms were discussed.

Until now, trisiloxane and its derivatives have been the only known superspreaders; however, as was mentioned in the Introduction, they cannot be used in food, pharmaceuticals, or other industries. The below experimental research was conducted to investigate the new synergetic composition of surfactants that are capable of improving the wetting properties of aqueous formulations and providing fast spreading over hydrophobic substrates. It can also shed light on the parameters affecting the rate of spreading and possible mechanisms enabling the fast spreading of surfactant solutions on hydrophobic surfaces.

It is important to notice that the affinity of a surfactant for the liquid/air and solid/liquid interface can be different because of the different chemical composition of these interfaces. Therefore, combining surfactants of a different nature can result in a synergetic effect providing much better wetting properties of mixed solutions as compared to solutions of individual surfactants.[76]

In ref 77, a synergetic mixture of two surfactants was investigated. This mixture showed partial wetting behavior on a hydrophobic substrate, silanized glass. The contact angle of pure aqueous droplets on this substrate was 102 ± 3°. The substrate was prepared according to the protocol described in ref 78. The surfactants under study were Zonyl FSN-100 (DuPont), fluorosurfactant, and octaethylene glycol monododecylether $C_{12}(EO)_8$ (>98%, Sigma). It was possible to vary the contact angle of aqueous solution by varying the ratio of the surfactants in the mixture and thus to study the dependence of spreading kinetics on the equilibrium contact angle. Concentrations above the CAC were used, and the contact angle of solutions of individual surfactants decreased very slowly with concentration in the studied range of concentrations.

Despite the large difference in the equilibrium surface tension (at concentrations above the CAC, the surface tension of $C_{12}(EO)_8$ was ∼35.3 mN/m vs ∼21.9 mN/m for Zonyl), the aqueous solutions of these surfactants have very similar contact angle values on silanized glass (52−57° for Zonyl and 54−55° for $C_{12}(EO)_8$ in the studied range of concentrations).[77] The most probable reason for that is the better adsorption of hydrocarbon surfactant $C_{12}(EO)_8$ on the hydrocarbon substrate, salinized glass.[65] Indeed, the measurement of the interfacial tension of aqueous solutions of these surfactants with a liquid hydrocarbon, heptane, has given values of about 3.4 mN/m for $C_{12}EO_8$ and 8.5 mN/m for Zonyl.[77]

After mixing, Zonyl adsorbs preferably on the liquid/air interface, whereas $C_{12}EO_8$ prefers the solid/liquid interface, resulting in considerably smaller values of the contact angle, i.e., better wetting, for mixtures (Figure 15).

It was found[77] that the spreading exponent for surfactant solutions with respect to partial wetting behavior (in contrast to complete wetting) is smaller than that for pure liquids and decreases with the increase in the contact angle. The maximum spreading rate was observed for the mixture demonstrating the lowest value of the contact angle (Figure 16).

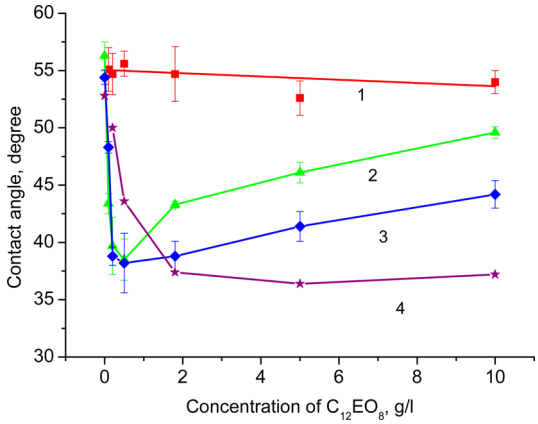

Figure 15. Contact angle on silanized glass for the $C_{12}EO_8$ surfactant solution (1) and v/v = 1:1 mixtures with Zonyl FSN-100 solutions at concentrations of 0.5 (2), 1 (3), and 10 g/L (4). Reproduced with permission from ref 77. Copyright 2015 Elsevier B.V.

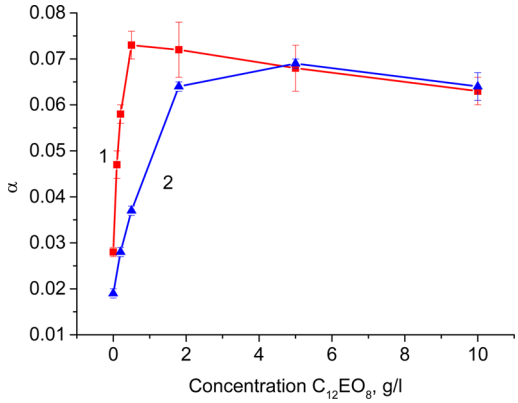

Figure 16. Spreading exponent, α, for mixed solutions depending on the concentration of $C_{12}EO_8$. Concentrations of Zonyl FSN-100: 1−0.5 and 2−10 g/L. Reproduced with permission from ref 77. Copyright 2015 Elsevier B.V.

A decrease in the spreading exponent for surfactant solutions in the case of partial wetting was also observed for other surfactants.[3] This means that the rate of spreading of the surfactant solution is limited by a process that is absent in pure liquids. It can be assumed that the process of interest is surfactant adsorption. It can be the adsorption kinetics at the liquid/air and solid/liquid interface or, as proposed in ref 1, the adsorption of surfactant molecules on a solid/air interface in front of the three-phase contact line that facilitates the wetting process. In conclusion to this part, it was found in ref 77 that the rate of spreading of mixed solutions depends on the mixing protocol: premixed solutions spread faster than in the case when a drop of one of the individual solutions is placed on top of the drop of another solution matter in which the drop was applied first. This finding shows that the surfactant redistribution in the drop and thus the adsorption kinetics affect the rate of spreading. Therefore, equilibrium values of surface and interfacial tension and dynamic effects can be responsible for superspreading behavior. Also, strong adsorption on both solid/liquid and vapor/liquid interfaces is not enough to provide the superspreading behavior.

DOI: 10.1021/acs.langmuir.6b04094
Langmuir 2017, 33, 4367−4385

A stronger synergetic effect than discussed above was observed for the mixed solutions of anionic and cationic surfactants.[79−81] Such mixtures show superspreading behavior on a polyethylene film.[79−81] The synergetic effect in this case is due to charge neutralization, enabling closer packing of surfactant molecules in the adsorbed layer. A series of cationic surfactants and a series of anionic surfactants were tested, and the best performing pair was selected. This best performing mixture was cationic surfactant dodecyltrimethylammonium bromide when mixed with anionic sodium octanesulfonate (Figure 17).[81] For this

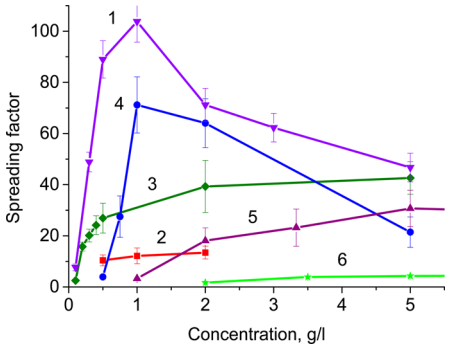

Figure 17. Spreading factors of solutions of (1) superspreader BT-278 and a v/v = 1:1 mixture of dodecyltrimethylammonium bromide with (2) sodium dodecanesulfonate, (3) sodium decanesulfonate, (4) sodium octanesulfonate, (5) sodium heptanesulfonate, and (6) sodium hexanesulfonate. Reproduced with permission from ref 81. Copyright 2015 Elsevier B.V.

synergetic mixture, the spreading factor, displaying the effectiveness of surfactant in promoting the spreading, is close to that of trisiloxane superspreader BREAK-THRU S 278, BT-278 (Evonik) (Figure 17).[81] The spreading factor is the ratio of the spread area of surfactant solution to the spread area of a pure water drop of similar volume.

However, the spreading performance of mixed solutions of cationic and anionic surfactants can be suppressed by the low solubility of a mixture. If the solubility limit is below the CAC value, then the formed crystals both essentially lower the concentration of free molecules in the mixed solution and decrease the solution spreadability, and the formed crystals can coadsorb on the liquid/air interface, retarding it and slowing down the spreading. An example is given in ref 80. When the solutions of dodecyltrimethylammonium bromide and sodium decanesulfonate are mixed in a v/v = 1:1 proportion and the concentration of the mixture is above the CAC, the mixture first spreads completely on a polyethylene film. However, the solubility of the mixture is below the CAC; therefore, the formation of crystals starts immediately after mixing. The crystallization proceeds slowly and initially does not influence the spreading performance. However, in approximately 30 s crystallization decreases the concentration of free surfactant molecules in the solution below the CAC. As a result, the conditions for complete wetting are not fulfilled anymore and the solution reassembles back into the drop, which wets the substrate only partially.

Despite the same spreading exponent, $\alpha = 0.5$, the spreading of the mixtures of dodecyltrimethylammonium bromide and sodium octanesulfonate occurs much more slowly than that of superspreader BT-278 (Figure 18).[81] That means that the mechanism of spreading responsible for the exponent value is the same for these solutions, whereas some characteristics of the

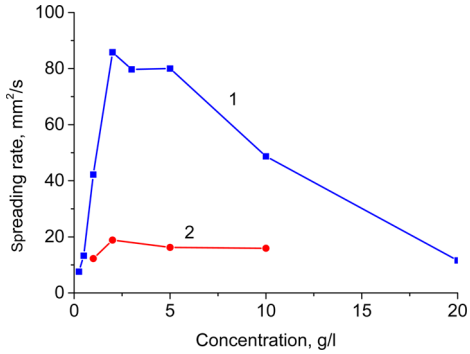

Figure 18. Spreading rate vs concentration for (1) superspreader BT-278 and (2) v/v = 1:1: mixed solutions of dodecyltrimethylammonium bromide and sodium octanesulfonate. Reproduced with permission from ref 81. Copyright 2015 Elsevier B.V.

surfactants included in the preexponential factor are different. The similar spreading factors of these solutions (i.e., similar final spreading areas) are due to a longer time of spreading for the mixed solution.

A comparative study of solutions of two surfactants was undertaken to identify a key factor responsible for the difference in the spreading rate: superspreader BT-278 and nonionic surfactant triethylene glycol monodecyl ether, $C_{10}EO_3$.[82] The wetting performance of the solutions of the latter surfactant was worse as compared to that of the superspreader: $C_{10}EO_3$ solutions demonstrated only partial wetting on a polyethylene film. Therefore, the spreading experiments were performed on the less hydrophobic substrate, a polyvinylidene fluoride (PVDF) film, and the effect of roughness was used to improve the wetting performance of $C_{10}EO_3$ solutions.[60,83]

In agreement with the literature data,[61] it was found in ref 82 that the spreading rate depends on the surfactant concentration with a maximum at moderate concentrations of 1−3 g/L. This dependency is in agreement with the importance of Marangoni convection for the mechanism of superspreading.[69−71] Indeed, at small concentrations of surfactant the surface tension at the leading edge of spreading is far from equilibrium, but it is also far from equilibrium in the other parts of the spreading drop because of the slow surfactant transfer to the expanding surface. Therefore, the surface tension gradients driving the spreading are small, especially taking into account that the surface tension changes slowly at small values of subsurface concentration. The involved surface tension gradients initially increase with concentration because the surface tension far from the spreading edge equilibrates faster. But at a certain concentration, the gradients begin to decrease because of faster adsorption at the leading edge of spreading. A more detailed discussion of the effect of concentration on the rate of spreading due to the Marangoni effect can be found in refs 69−71. A comparison of the data presented in Figure 19 shows that the spreading rates of solutions of BT-278 are higher than those of $C_{10}EO_3$ solutions at all concentrations studied. Hence, this difference in the rate of spreading is not a concentration effect.

The rate of spreading was compared to the rate of surface/bulk equilibration of corresponding solutions as measured by dynamic surface tension. It was found in ref 82 that the solutions of $C_{10}EO_3$ demonstrate slower spreading (Figure 19) but faster equilibration between the bulk and surface (Figure 20). Therefore, the rate of equilibration (dynamic surface tension) can be considered to be one of the important parameters affecting the kinetics of spreading. Because slower equilibration assumes the

DOI: 10.1021/acs.langmuir.6b04094
Langmuir 2017, 33, 4367−4385

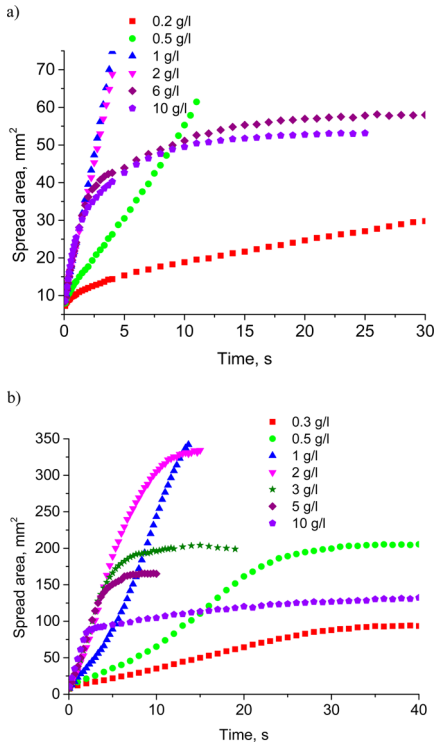

Figure 19. Spreading kinetics of (a) $C_{10}EO_3$ and (b) BT-278 solutions on a PVDF film. Reproduced with permission from ref 82. Copyright 2016 The Royal Society of Chemistry.

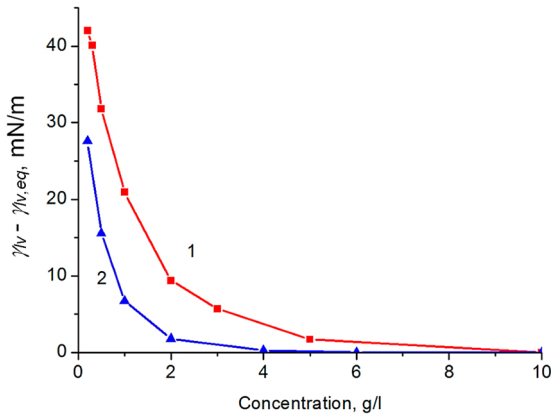

Figure 20. Deviation of the surface tension from its equilibrium value on a time scale of 0.1 s: (1) BT-278 and (2) $C_{10}EO_3$. Reproduced with permission from ref 82. Copyright 2016 The Royal Society of Chemistry.

possibility of the development of essential Marangoni stresses in the system, the results obtained in ref 82 confirmed that Marangoni flow is an essential part of the mechanism of surfactant-enhanced spreading.

Hence, a consideration presented in this part shows that the kinetics of adsorption plays an important role, as does the Marangoni phenomenon, and future research in this direction is rather promising.

Kinetics of Spreading of Surfactant Solutions over Hair. The interaction of liquids with human hair occurs not only during washing by the utilization of hair care products such as shampoos, conditioners, and hair colorants but also in contact with atmospheric moisture.[84,85] The contact angle measurement is a simple method to check the wetting behaviors of different liquids on hair. A majority of the studies available in the literature concentrate on the interaction of a single hair fiber (dry or wet) with various liquids.[84−88] However, the wetting of dry hair tresses with polymer solutions has been largely unexplored until now. Below an investigation of the wetting and spreading of polymer solutions on dry tresses of hair is briefly discussed.[89]

Hair is a natural fiber consisting of a core (cortex and medulla) covered with overlapping cuticle cells. The most important for wetting is the outer surface of the cuticle, which, on undamaged hair, is covered by a covalently attached monolayer of fatty acid (18-methyle-icosanic acid), thus making the fiber slightly hydrophobic.[90−92]

The experiments were conducted using two polyacrylate polymers, Aculyn 22 and Aculyn 33, which are broadly applied by the hair care industry, for example, in the production of hair colorants and hair styling gels.[89] Aqueous solutions of these polymers are viscous, and they show shear-thinning non-Newtonian behavior.[93,94]

Aculyn 22 (A22 below) is a hydrophobically modified anionic alkali-soluble polymeric emulsion, and Aculyn 33 (A33 below) is an anionic alkali-soluble polymer emulsion that is lightly cross-linked.[95,96] Both emulsions may contain some surfactant (sodium dodecyl sulfate). The influence of surfactant on wetting on hair was separately investigated. General structures of the polymers are presented in ref 93. The polymers are soluble in water at high pH (>7). Aqueous solutions of the polymers were made in the concentration range of 1.0−1.5% w/w. Sodium chloride (NaCl) and isopropyl alcohol (i-propanol, ipr-OH) were added to the solutions in the range of 0−1.5 M and at 0 or 1.67 M (10% w/w) concentration, respectively. Sodium dodecyl sulfate surfactant (SDS) was used at a concentration of 5 mM. The above compositions represent the formula that is commonly used in cosmetic applications, for example, in hair colorant products. The rheological properties of the studied solutions are presented in refs 93 and 94.

The details of experimental procedure can be found in ref 89. The hair tresses were secured in a special frame to provide as much hair alignment as possible for wetting measurements. The thickness of the tresses was sufficient to avoid contact of the investigated liquid with the frame material. There was some expected variation in the arrangement of individual hair fibers on the frame in the repeat experiments, leading to the increased standard error in the measurements. Measurements of the contact angle were performed on dry hair tresses. The contact angle, θ, the droplet volume, V, and the droplet base diameter, $2L$, were monitored as functions of time, t. The processing time was defined as the time during which the droplet remains on the hair tress. The initial contact angle was measured right after droplet deposition. The final (static advancing) contact angle was measured at the end of spreading when $2L$ reached a plateau. All measurements were made at 20 °C and 40% relative humidity, and the droplet volume was 2−3 μL. At least 10 repeat measurements were performed on hair tresses, and the error was in the range of 10−20% due to variations in the tress arrangement on the frame, as mentioned above.

The initial contact angle of a pure water droplet on hair is around 100°. It was found that there are three wetting regimes: (a) Cassie wetting, where liquid is sitting on the hair tress, without penetrating the tress, (b) Wenzel wetting, characterized by the penetration of liquid into the hair tress, and (c) the transition from Cassie to Wenzel wetting, after some critical contact angle is reached.

DOI: 10.1021/acs.langmuir.6b04094
Langmuir 2017, 33, 4367−4385

The dynamic contact angle and baseline diameter of the A22 polymer solution droplets on the hair tresses are presented in Figure 21. The initial contact angle on the hair tress for this

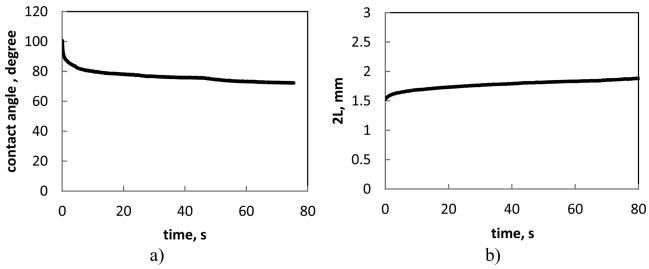

Figure 21. (a) Contact angle and (b) baseline diameter of an A22 1%, 0.3 M NaCl solution on a hair tress. Reproduced with permission from ref 89. Copyright 2015 Elsevier B.V.

polymer was about 100°. Spreading stopped after 10−20 s, and the contact angle had reached a value of around 75° (Figure 21). The droplets remained on the surface of the hair tress after the initial fast spreading stage. Following this, the total processing time (until the droplet disappearance) was around 2000 s. During this later stage, slow evaporation and possible imbibition of the solutions inside the hair tresses were observed. Similar behavior of the solutions of A22 with additives (SDS and i-prOH) was observed in most cases. The addition of SDS and i-prOH causes the droplet to spread faster, but the total processing time is similar.[89] This behavior could be attributed to the presence of a yield stress for A22 solutions, which was detected in previous publications.[93,95]

The initial contact angle of the A33 solutions on the hair tresses was about 100°. The first fast stage of spreading was completed after 15 s. The final contact angle at the end of spreading was around 60°. The total processing time, during which the droplet disappeared completely, was around 150 s (Figure 22).

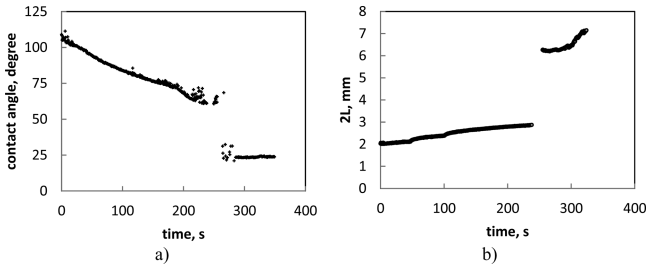

Figure 22. (a) Contact angle and (b) baseline diameter of an A33 1%, 0 M NaCl solution on a hair tress. Reproduced with permission from ref 89. Copyright 2015 Elsevier B.V.

Figure 22 shows that in the case of A33 solutions, where the contact angle reached the critical value (around 60°), fast penetration into the hair tress was observed. This resulted in a jump in the contact angle dependency on time and also the base diameter (Figure 22). This can be explained by the Cassie−Wenzel wetting transition, which is caused by filling the pores inside porous media (such as hair tress in the case) with liquid.[89,97−100] The schematic penetration of the liquid inside the porous media (hair tress) is presented in Figure 23. In the Cassie stage, liquid wetted only the first layer of fibers; however, in the Wenzel stage, liquid penetrated inside the hair tress. After the transition, capillary transport along the fibers is also possible.

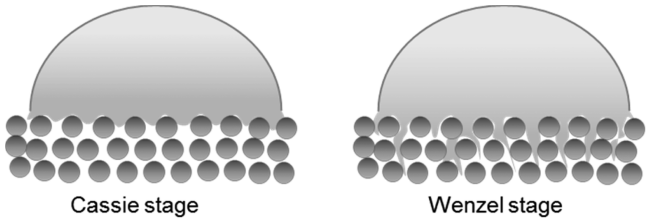

Figure 23. Behavior of a liquid droplet on a hair tress. In the Cassie stage, only first layer of fibers is wetted. In the Wenzel stage, liquid penetrates the hair. Reproduced with permission from ref 89. Copyright 2015 Elsevier B.V.

It was shown in refs 89, 97, and 98 that the condition for the wetting transition is to reach the critical contact angle, which was found to be around 60°. This condition is satisfied for the A33 solutions but is not satisfied for the A22 solution, with the latter forming a higher contact angle. This wetting transition of the solutions of A33 with various additives (SDS and i-prOH) was observed in most cases. These additives change the rheology of the solutions; however, this did not influence the presence of the wetting transition. However, because of the random hair arrangement the value of the critical contact angle fluctuates considerably.

The effects of i-propanol and SDS additives were also investigated. Both solvents and surfactants are capable of changing the surface tension and bulk rheology of the polymer solutions. i-Propanol and SDS were chosen because they are frequently used in cosmetics formulations. In the case of the A22 1%, 0.3 M, 10% ipr-OH solution on the hair tress, the initial and final contact angles were around 80° and in the range of 60−50 °, respectively. The spreading was very fast (1−4 s), but the total processing time was long, around 2400 s. The solution showed better spreading than the solution without alcohol but not better penetration. In the case of the A22 1%, 1.3 M, 10% ipr-OH solution, the droplet penetrated the hair tress just after deposition, which indicates that the initial contact angle was smaller than a critical value corresponding to the Cassie−Wenzel transition mentioned above and that penetration occurred immediately. An alcohol additive made the initial contact angle slightly smaller and the total processing time shorter in comparison to the solutions without alcohol.

The addition of 5 mM SDS to the A22 1%, 0.3 M solution resulted in slightly different wetting behavior on the hair. The initial and final contact angles were lower (90 and 50°, respectively) than those for the solutions without SDS, and the spreading time was longer. However, the total processing time was identical in both cases. The greatest effect of the SDS additive on the A33 solutions was the reduction in total processing time. Similar to A22, wetting properties of the A33 solutions were improved by the addition of SDS. Thus, the addition of SDS and i-propanol to the polymer solutions improved their spreading on hair.

■ CONCLUSIONS

It was shown in part 1 that all equilibrium and static advancing/receding contact angles on a smooth homogeneous solid surface can be calculated via disjoining/conjoining pressure isotherms. In spite of some qualitative experiments confirming the theory predictions, the precise calculation of all mentioned angles is impossible at the current stage of science in the area. The problem is in the possibility (or rather the impossibility) of a disjoining/conjoining pressure isotherm over the whole range of

DOI: 10.1021/acs.langmuir.6b04094
Langmuir 2017, 33, 4367−4385

thickness. There is only a limited range of flat liquid films where the disjoining/conjoining pressure can be measured: only in the range of (i) $\Pi(h) > 0$ (undersaturation) and (ii) flat films satisfying the stability condition, $\Pi'(h) < 0$. In the range of thickness where $\Pi(h) < 0$ (which correspond to oversaturation), currently there are no available experimental methods or range of thickness $\Pi'(h) > 0$ where unstable flat films are formed. More than that, inside the transition zone (where both capillary and surface forces are equally important) the liquid profile is not flat at all. There are only limited attempts to take this into account. Next, the surfaces considered in part 1 are ideal, without roughness, which is frequently not the case in real situations. There is not a single attempt to consider either equilibrium or hysteresis contact angles by taking into account the action of disjoining/conjoining pressure on rough surfaces.

In part 2, the deformation of soft solids under a liquid droplet was considered. It was proven that the deformation of soft solids is determined by the action of surface forces inside the transition zone. However, over many years of investigation of this process only a few papers have been published in this area (cited in part 2). That is, the basics of this phenomenon are to be understood. It was shown in part 2 that even in the case of equilibrium the deformation is more complex than was assumed in earlier investigations. Note that there is a substantial problem here: the experimental observation of equilibrium droplets on either nondeformable or deformable substrates is impossible because according to Kelvin's equation the droplets should be kept at equilibrium with oversaturated vapor for a prolonged period of time and the oversaturation should be kept constant with enormously high precision. This is currently beyond the experimental capabilities and is the reason that only static advancing/receding contact angles can be experimentally observed on either nondeformable or deformable substrates. A theory of the calculations of contact angle hysteresis was suggested only recently (part 1) on nondeformable solid substrates and has never been attempted in the case of deformable substrates. This is to be done in the future.

In part 3, the kinetics of spreading of blood droplets over a porous substrate was investigated. It is surprising that in spite of a large amount of practical experience accumulated in various areas of applications, sometimes the basics are still to be understood. An interesting example is blood spreading over porous substrates (part 3). It is obvious that blood is an enormously complex liquid. However, is this complexity important for the process of simultaneous spreading/imbibition over porous substrates? It turns out that from this point of view blood is a relatively simple power law shear-thinning liquid. This allowed the development of a spreading model, which was in reasonable agreement with the experimental data.

The phenomenon of superspreading has attracted the attention of the scientific community for a long time. However, the physical mechanism of suprspreading is to be understood in spite of much effort in this area. The aim of the experimental research presented in part 4 was to investigate new synergetic compositions of surfactants that are capable of providing fast spreading over hydrophobic substrates as well as to identify possible mechanisms of superspreading and effective parameters for rate spreading. Is a strong adsorption of surfactants on both liquid−vapor and solid−liquid interfaces the physical phenomenon providing the superspreading conditions? A synergetic mixture of surfactants investigated in part 4 gives a negative answer to this question. However, an investigation of mixtures confirms that the rate of adsorption and the Marangoni phenomenon are still possible candidates for the superspreading mechanism. We still believe that the caterpillar motion at the moving three-phase contact line reduces the friction at the moving apparent three-phase contact line, and this physical phenomenon contributes considerably to superspreading. However, it is to be proven experimentally.

The application of spreading processes to the wetting of hair tresses was presented in part 5. It was shown that the wetting transition determines the possible wetting of hair. The critical contact angle was found, and it agrees with other investigations in this area.

AUTHOR INFORMATION

Corresponding Author

*E-mail: V.M.Starov@lboro.ac.uk.

ORCID

Victor Starov: 0000-0003-0814-8870

Notes

The authors declare no competing financial interest.

Biographies

Omid Arjmandi-Tash graduated with a B.Sc. (Eng) degree (2010) in chemical engineering from the University of Tabriz, Iran, and he received his M.Sc. (Eng) degree (2013) in chemical engineering from the University of Tehran, Iran. In 2014, he joined the Department of Chemical Engineering at Loughborough University, U.K. as a Marie Curie Early Stage Researcher and Ph.D. candidate. He is currently working on several aspects of the interaction of droplets and foams with porous substrates with a focus on droplets of non-Newtonian liquids and foams of Newtonian surfactants and non-Newtonian polymeric solutions.

Nina M. Kovalchuk earned her Ph.D. in material science in 1996. She moved to the area of colloid and interface science in 1998 and worked as a postdoctoral research scientist at the Institute of Biocolloid Chemistry,

DOI: 10.1021/acs.langmuir.6b04094
Langmuir 2017, 33, 4367−4385

Kiev, Ukraine, the Max-Planck Institute of Colloids and Surfaces, Potsdam, Germany, and the Department of Chemical Engineering, Loughborough University, U.K. (Prof Starov's group). Currently, she is a research fellow at the School of Chemical Engineering, University of Birmingham, U.K. Her research interests are in the areas of adsorption dynamics and the effect of surfactants on multiphase flows (surfactant enhanced spreading and superspreading, formation and coalescence of drops on the macroscale and in microfluidic devices, and instabilities due to surfactant transfer), and the stability and dynamics of foams, suspensions, and emulsions.

Anna Trybala earned her Ph.D. in physical chemistry in 2011 from the Institute of Catalysis and Surface Chemistry, Polish Academy of Sciences, Cracow, Poland. In October 2011, Anna started working as a research associate in the Chemical Engineering Department at Loughborough University, after which, in October 2015, she was appointed as a lecturer. Her major research interests are in the areas of applications of the kinetics of wetting and spreading, colloid engineering, and foams. She is studying transport processes between foams and porous substrates in cosmetic, pharmaceutical, and household formulations. She is interested in foams formed by Newtonian surfactants solutions and non-Newtonian surfactant–polymer mixtures.

Igor V. Kuchin obtained his Ph.D. degree (2002) in chemical engineering from Boreskov Institute of Catalysis, Russia. Since 2005, he has been a senior scientist at the Institute of Physical Chemistry and Electrochemistry, Russian Academy of Sciences. In 2013 and 2014, he was a research associate at Loughborough University, U.K. His research activity is focused on mathematical modeling and computer simulation in colloid and interface science: interfacial phenomena, wetting processes, surface interactions, thin liquid films, and the rheology and dynamics of colloid and disperse systems.

Victor Starov, Ph.D., D.Sc., Fellow of the Royal Society of Chemistry, and professor. Victor Starov is a professor in the Department of Chemical Engineering, Loughborough University, U.K. For more than 30 years, Victor has been involved in research related to the kinetics of wetting and spreading. He has published more than 300 scientific papers and has been a member of editorial boards of 10 journals. For more information, see ref 101.

■ ACKNOWLEDGMENTS

This research was supported by European Science Foundation Marie Curie ITN grants MULTIFLOW and CoWet; the Engineering and Physical Research Council, UK grants EP/J010596/1 and EP/D077869/1; Procter & Gamble, USA; and the European Space Agency under grants FASES, PASTA, and MAP EVAPORATION.

■ NOMENCLATURE

a, slope of the disjoining/conjoining pressure isotherm defined in Figure 5,
A_H, Hamaker constant
c_0, electrolyte concentration
F, Faraday's constant
h, film thickness, equilibrium liquid profile, droplet height
h_β, metastable equilibrium film thickness
h_e, stable equilibrium film thickness
h_s, local deformation of the substrate
h_{se}, local deformation of the substrate under the action of ambient pressure
h_u, h_{uu}, unstable film thicknesses
h^*, scale of the droplet height
H, drop height at the drop apex, half-width of a two-dimensional capillary
k, flow consistency index
K, elasticity coefficient
K_n, permeability of the porous layer
K_1, parameters related to the magnitude of the short-range structural forces
K_2, parameters related to the magnitude of the long-range structural forces
l, radius of the wetted area inside the porous substrate
$\bar{l}$, dimensionless radius of the wetted area inside the porous substrate
l^*, radius of wetted region at the end of the process
L, radius of the droplet base
L_{ad}, maximum radius of the droplet base in a partial wetting case
L_m, maximum radius of the droplet base in a complete wetting case

DOI: 10.1021/acs.langmuir.6b04094
Langmuir 2017, 33, 4367–4385

L^*, scale of the droplet base
$\bar{L}$, dimensionless droplet base
L_1, length from the origin of a droplet to the point where the influence of the surface forces comes into play (Figure 4)
m, porosity of the porous layer
n, flow behavior index
p, vapor pressure over a curved interface
p_c, capillary pressure inside the pores of the porous layer
p_s, saturated vapor pressure over a flat liquid surface
P, nonequilibrium pressure, applied pressure from a droplet to its substrate
P_e, excess (equilibrium) pressure
P_l, pressure inside the liquid
P_v, pressure in the ambient vapor
P_1, P_2, parameters of the disjoining/conjoining pressure isotherm defined in Figure 5
r, radial coordinate
r_e, radius of the spherical meniscus/cap
R, universal gas constant
S, area of the liquid−air interface
S_s, area of the solid−liquid interface
x, coordinate axis
t, time
T, temperature
t_{ad}, time when the advancing contact angle is reached
t_o, parameter of the disjoining/conjoining pressure isotherm defined in Figure 5
t_m, time when the radius of the droplet base reaches its maximum value in a complete wetting case
t_r, time when the receding contact angle is reached
t_0, duration of the initial fast stage of spreading
t_1, range of surface forces action
t^*, time of complete imbibition
$\bar{t}$, dimensionless time
y, coordinate normal to the liquid−air interface
v_m, molar volume of the liquid
v_+, rate of expansion of the drop base
v_-, rate of shrinkage of the drop base
V, droplet volume
V_a, volume of a flat (two-dimensional) droplet
V_0, initial droplet volume
z, coordinate axis

Greek Symbols

α, spreading exponent
α_n, coefficient in eq 23
γ_{lv}, liquid−vapor interfacial tension
γ_{sl}, solid−liquid interfacial tension
γ_{sv}, solid/vapor interfacial tension
$\dot{\gamma}$, shear rate
Δ, thickness of the thin porous substrate
ε, dielectric constant of water
ε_0, dielectric constant of vacuum
η, viscosity
θ, contact angle
θ_{ad}, advancing contact angle
θ_e, equilibrium contact angle
θ_f, final contact angle in a complete wetting case
θ_m, contact angle at the maximum droplet base radius in the complete wetting case
θ_r, receding contact angle
$\bar{\theta}$, dimensionless contact angle
λ, constant in eq 23
λ_1, parameter related to the characteristic length of the short-range structural forces
λ_2, parameter related to the characteristic length of the long-range structural forces
ξ, spreading coefficient
II, disjoining/conjoining pressure isotherm
Π_E, electrostatic component of disjoining/conjoining pressure
Π_M, molecular or van der Waals component of disjoining/conjoining pressure
Π_S, structural component of disjoining/conjoining pressure
σ_h, surface charge density for the liquid/vapor interface
σ_s, surface charge density for the solid/liquid interface
φ, dimensionless electric potential
Φ, excess free energy of a droplet
$\Phi_{e,film}$, excess free energy of a flat equilibrium liquid film

REFERENCES

(1) Starov, V.; Velarde, M.; Radke, C. *Wetting and Spreading Dynamics*; Surfactant Science Series; CRC Press, 2007; Vol. *138*, pp 1−544.
(2) Derjaguin, B. V.; Churaev, N. V.; Muller, V. M. *Surface Forces*; Consultants Bureau-Plenum: New York, 1987.
(3) Ivanova, N. A.; Starov, V. M. Wetting of Low Free Energy Surfaces by Aqueous Surfactant Solutions. *Curr. Opin. Colloid Interface Sci.* **2011**, *16*, 285−291.
(4) Chibowski, E. Surface Free Energy of a Solid from Contact Angle Hysteresis. *Adv. Colloid Interface Sci.* **2003**, *103*, 149−172.
(5) Extrand, C. W.; Kumagai, Y. An Experimental Study of Contact Angle Hysteresis. *J. Colloid Interface Sci.* **1997**, *191*, 378−383.
(6) Extrand, C. W. Water Contact Angles and Hysteresis of Polyamide Surfaces. *J. Colloid Interface Sci.* **2002**, *248*, 136−142.
(7) Romanov, E. A.; Kokorev, D. T.; Churaev, N. V. Effect of Wetting Hysteresis on State of Gas Trapped by Liquid in a Capillary. *Int. J. Heat Mass Transfer* **1973**, *16*, 549−554.
(8) Platikanov, D.; Yampolskaya, G. P.; Rangelova, N.; Angarska, Zh.; Bobrova, L. E.; Izmailova, V. N. Free Black Films of Proteins. Thermodynamic Parameters. *Colloid J. (USSR)* **1981**, *43*, 177−180.
(9) Rangelova, N. I.; Izmailova, V. N.; Platikanov, D. N.; Yampol'skaya, G. P.; Tulovskaya, S. D. Free Black Films of Proteins: Dynamic Hysteresis of the Contact Angle (Film-Bulk Liquid) and the Rheological Properties of Adsorption Layers. *Colloid J. (USSR)* **1990**, *52*, 442−447.
(10) Platikanov, D.; Nedyalkov, M.; Petkova, V. Phospholipid Black Foam Films: Dynamic Contact Angles and Gas Permeability of DMPC Bilayer Films. *Adv. Colloid Interface Sci.* **2003**, *100−102*, 185−203.
(11) Kuchin, I.; Starov, V. Hysteresis of the Contact Angle of a Meniscus inside a Capillary with Smooth, Homogeneous Solid Walls. *Langmuir* **2016**, *32*, 5333−5340.
(12) Kuchin, I.; Starov, V. Hysteresis of Contact Angle of Sessile Droplets on Smooth Homogeneous Solid Substrates via Disjoining/Conjoining Pressure. *Langmuir* **2015**, *31*, 5345−5352.
(13) Churaev, N. V.; Sobolev, V. D. Wetting of Low-Energy Surfaces. *Adv. Colloid Interface Sci.* **2007**, *134−135*, 15−23.
(14) Rowlinson, J. S.; Widom, B. *Molecular Theory of Capillarity*; Clarendon Press, 1982.
(15) Churaev, N. V.; Sobolev, V. D.; Starov, V. M. Disjoining Pressure of Thin Nonfreezing Interlayers. *J. Colloid Interface Sci.* **2002**, *247*, 80−83.
(16) Frumkin, A. N. Phenomena of Wetting and Adhesion of Bubbles. *Zh. Fiz. Khim.* **1938**, *12*, 337−345.
(17) Churaev, N. V.; Sobolev, V. D. Prediction of Contact Angles on the Basis of the Frumkin-Derjaguin Approach. *Adv. Colloid Interface Sci.* **1995**, *61*, 1−16.
(18) Gu, Y. Drop Size Dependence of Contact Angles of Oil Drops on a Solid Surface in Water. *Colloids Surf., A* **2001**, *181*, 215−224.
(19) Churaev, N. V.; Setzer, M. J.; Adolphs, J. Influence of Surface Wettability on Adsorption Isotherms of Water Vapor. *J. Colloid Interface Sci.* **1998**, *197*, 327−333.

DOI: 10.1021/acs.langmuir.6b04094
Langmuir 2017, 33, 4367−4385

(20) Mack, G. L. The Determination of Contact Angles from Measurements of the Dimensions of Small Bubbles and Drops. I. The Spheroidal Segment Method for Acute Angles. *J. Phys. Chem.* **1936**, *40*, 159−167.
(21) Veselovsky, V. S.; Pertsev, V. N. Adhesion of the Bubbles to Solid Surfaces. *J. Phys. Chem. (USSR)* **1936**, *8*, 245−259 (in Russian).
(22) Young, T. An Essay on the Cohesion of Fluids. *Philos. Trans. R. Soc. London* **1805**, *95*, 65−87.
(23) Rusanov, A. On the Thermodynamics of Deformable Solid Surfaces. *J. Colloid Interface Sci.* **1978**, *63*, 330−345.
(24) Rusanov, A. Theory of Wetting of Elastically Deformed Bodies. 1. Deformation with a Finite Contact-angle. *Colloid J. (USSR)* **1975**, *37*, 614−622.
(25) Rusanov, A. Theory of Wetting of Elastically Deformed Bodies. 2. Equilibrium Conditions and Work of Deformation with a Finite Contact Angle. *Colloid J. (USSR)* **1975**, *37*, 623−628.
(26) Shanahan, M. E. R. The Spreading Dynamics of a Liquid Drop on a Viscoelastic Solid. *J. Phys. D: Appl. Phys.* **1988**, *21*, 981−985.
(27) Shanahan, M. E. R.; de Gennes, P. G. The Ridge Produced by a Liquid near the Triple Line Solid Liquid Fluid. *C. R. Acad. Sci., Ser. II* **1986**, *302*, 517−521.
(28) Carre, A.; Shanahan, M. E. R. Viscoelastic Braking of a Running Drop. *Langmuir* **2001**, *17*, 2982−2985.
(29) Schulman, R. D.; Dalnoki-Veress, K. Liquid Droplets on a Highly Deformable Membrane. *Phys. Rev. Lett.* **2015**, *115*, 206101.
(30) Lubbers, L. A.; Weijs, J. H.; Botto, L.; Das, S.; Andreotti, B.; Snoeijer, J. H. Drops on Soft Solids: Free Energy and Double Transition of Contact Angles. *J. Fluid Mech.* **2014**, *747*, 10.1017/jfm.2014.152.
(31) Derjaguin, B. V.; Starov, V. M.; Churaev, N. V. Pressure on a Wetting Perimeter. *Colloid J. (USSR)* **1982**, *44*, 770−775.
(32) White, L. R. The Contact Angle on an Elastic Substrate. 1. The Role of Disjoining Pressure in the Surface Mechanics. *J. Colloid Interface Sci.* **2003**, *258*, 82−96.
(33) Gielok, M.; Lopes, M.; Bonaccurso, E.; Gambaryan-Roisman, T. Droplet on an Elastic Substrate: Finite Element Method Coupled with Lubrication Approximation. *Colloids Surf., A* **2016**, in press, doi:10.1016/j.colsurfa.2016.08.001.
(34) Ahmed, G.; Kalinin, V. V.; Arjmandi-Tash, O.; Starov, V. M. Equilibrium of Droplets on a Deformable Substrate: Influence of Disjoining Pressure. *Colloids Surf., A* **2016**, in press, doi:10.1016/j.colsurfa.2016.06.057.
(35) Winkler, E. *Die Lehre von der Elastizität und Festigkeit (The Theory of Elasticity and Stiffness)*; H. Dominicus: Prague, 1867.
(36) Kerr, A. D. Elastic and Viscoelastic Foundation Models. *J. Appl. Mech.* **1964**, *31*, 491−498.
(37) Churaev, N. V.; Starov, V. M.; Derjaguin, B. V. The Shape of the Transition Zone between a Thin Film and Bulk Liquid and the Line Tension. *J. Colloid Interface Sci.* **1982**, *89*, 16−24.
(38) Starov, V.; Tyatyushkin, A.; Velarde, M.; Zhdanov, S. Spreading of Non-Newtonian Liquids over Solid Substrates. *J. Colloid Interface Sci.* **2003**, *257*, 284−290.
(39) Betelu, S.; Fontelos, M. A. Capillarity Driven Spreading of Circular Drops of Shear-Thinning Fluid. *Math. Comput. Model.* **2004**, *40*, 729−734.
(40) Betelu, S.; Fontelos, M. A. Capillarity Driven Spreading of Power-Law Fluids. *Appl. Math. Lett.* **2003**, *16*, 1315−1320.
(41) Wang, X.; Lee, D.; Peng, X.; Lai, J. Spreading Dynamics and Dynamic Contact Angle of Non-Newtonian Fluids. *Langmuir* **2007**, *23*, 8042−8047.
(42) Liang, Z.; Wang, X.; Duan, Y.; Min, Q. Energy-Based Model for Capillary Spreading of Power-Law Liquids on a Horizontal Plane. *Colloids Surf., A* **2012**, *403*, 155−163.
(43) Wei, Y.; Rame, E.; Walker, L.; Garoff, S. Dynamic wetting with viscous Newtonian and non-Newtonian fluids. *J. Phys.: Condens. Matter* **2009**, *21*, 464126.
(44) Liang, Z.; Wang, X.; Duan, Y.; Min, Q.; Wang, C.; Lee, D. Dynamic Wetting of Non-Newtonian Fluids: Multicomponent Molecular-Kinetic Approach. *Langmuir* **2010**, *26*, 14594−14599.
(45) Alleborn, N.; Raszillier, H. Spreading and Sorption of a Droplet on a Porous Substrate. *Chem. Eng. Sci.* **2004**, *59*, 2071−2088.
(46) Kumar, S. M.; Deshpande, A. P. Dynamics of Drop Spreading on Fibrous Porous Media. *Colloids Surf., A* **2006**, *277*, 157−163.
(47) Starov, V.; Zhdanov, S.; Kosvintsev, S.; Sobolev, V.; Velarde, M. Spreading of Liquid Drops Over Porous Substrates. *Adv. Colloid Interface Sci.* **2003**, *104*, 123−158.
(48) Bou-Zeid, W.; Brutin, D. Effect of Relative Humidity on the Spreading Dynamics of Sessile Drops of Blood. *Colloids Surf., A* **2014**, *456*, 273−285.
(49) Brutin, D.; Sobac, B.; Nicloux, C. Influence of Substrate Nature on the Evaporation of a Sessile Drop of Blood. *J. Heat Transfer* **2012**, *134*, 061101.
(50) Brutin, D.; Sobac, B.; Loquet, B.; Sampol, J. Pattern Formation in Drying Drops of Blood. *J. Fluid Mech.* **2011**, *667*, 85−95.
(51) Sobac, B.; Brutin, D. Structural and Evaporative Evolutions in Desiccating Sessile Drops of Blood. *Phys. Rev. E* **2011**, *84*, 011603.
(52) Chao, T. C.; Trybala, A.; Starov, V.; Das, D. B. Influence of Haematocrit Level on the Kinetics of Blood Spreading on Thin Porous Medium during Dried Blood Spot Sampling. *Colloids Surf., A* **2014**, *451*, 38−47.
(53) Chao, T. C.; Arjmandi-Tash, O.; Das, D. B.; Starov, V. M. Spreading of Blood Drops Over Dry Porous Substrate: Complete Wetting Case. *J. Colloid Interface Sci.* **2015**, *446*, 218−225.
(54) Chao, T. C.; Arjmandi-Tash, O.; Das, D. B.; Starov, V. M. Simultaneous Spreading and Imbibition of Blood Droplets over Porous Substrates in the Case of Partial Wetting. *Colloids Surf., A* **2016**, *505*, 9−17.
(55) Meesters, R. J.; Hooff, G. P. State-of-the-Art Dried Blood Spot Analysis: An Overview of Recent Advances and Future Trends. *Bioanalysis* **2013**, *5*, 2187−2208.
(56) Stoebe, T.; Hill, R. M.; Ward, M. D.; Davis, H. T. Enhanced Spreading of Aqueous Films Containing Ionic Surfactants on Solid Substrates. *Langmuir* **1997**, *13*, 7276−7281.
(57) Stoebe, T.; Lin, Z.; Hill, R. M.; Ward, M. D.; Davis, H. T. Enhanced Spreading of Aqueous Films Containing Ethoxylated Alcohol Surfactants on Solid Substrates. *Langmuir* **1997**, *13*, 7270−7275.
(58) Stoebe, T.; Lin, Z.; Hill, R. M.; Ward, M. D.; Davis, H. T. Surfactant-enhanced Spreading. *Langmuir* **1996**, *12*, 337−344.
(59) Ananthapadmanabhan, K. P.; Goddard, E. D.; Chandar, P. A Study of the Solution, Interfacial and Wetting Properties of Silicone Surfactants. *Colloids Surf.* **1990**, *44*, 281−297.
(60) Lin, Z.; Hill, R. M.; Davis, H. T.; Ward, M. D. Determination of Wetting Velocities of Surfactant Superspreaders with the Quartz Crystal Microbalance. *Langmuir* **1994**, *10*, 4060−4068.
(61) Hill, R. M. Superspreading. *Curr. Opin. Colloid Interface Sci.* **1998**, *3*, 247−254.
(62) Rafai, S.; Sarker, D.; Bergeron, V.; Meunier, J.; Bonn, D. Superspreading: Aqueous Surfactant Drops Spreading on Hydrophobic Surfaces. *Langmuir* **2002**, *18*, 10486−10488.
(63) Radulovic, J.; Sefiane, K.; Shanahan, M. E. R. Dynamic of Trisiloxane Wetting: Effects of Diffusion and Surface Hydrophobicity. *J. Phys. Chem. C* **2010**, *114*, 13620−13629.
(64) Venzmer, J. Superspreading − 20 Years of Physico-chemical Research. *Curr. Opin. Colloid Interface Sci.* **2011**, *16*, 335−343.
(65) Kovalchuk, N. M.; Trybala, A.; Starov, V.; Matar, O.; Ivanova, N. Fluoro- vs Hydrocarbon Surfactants: Why Do They Differ in Wetting Performance? *Adv. Colloid Interface Sci.* **2014**, *210*, 65−71.
(66) Svitova, T.; Hill, R. M.; Smirnova, Yu.; Stuermer, A.; Yakubov, G. Wetting and Interfacial Transitions in Dilute Solutions of Trisiloxane Surfactants. *Langmuir* **1998**, *14*, 5023−5031.
(67) Theodorakis, P.; Muller, E. A.; Craster, R. V.; Matar, O. K. Superspreading: Mechanisms and Molecular Design. *Langmuir* **2015**, *31*, 2304−2309.
(68) Karapetsas, G.; Craster, R. V.; Matar, O. K. On Surfactant-Enhanced Spreading and Superspreading of Liquid Drops on Solid Surfaces. *J. Fluid Mech.* **2011**, *670*, 5−37.

DOI: 10.1021/acs.langmuir.6b04094
Langmuir 2017, 33, 4367−4385

(69) Nikolov, A.; Wasan, D.; Chengara, A.; Koczo, K.; Policello, G. A.; Kolossvary, I. Superspreading Driven by Marangoni Flow. *Adv. Colloid Interface Sci.* **2002**, *96*, 325−338.
(70) Chengara, A.; Nikolov, A.; Wasan, D. Surface Tension Gradient Driven Spreading of Trisiloxane Surfactant Solution on Hydrophobic Solid. *Colloids Surf., A* **2002**, *206*, 31−39.
(71) Nikolov, A.; Wasan, D. Superspreading Mechanisms: An Overview. *Eur. Phys. J.: Spec. Top.* **2011**, *197*, 325−341.
(72) Frank, B.; Garoff, S. Surfactant self-assembly near contact lines: control of advancing surfactant solutions. *Colloids Surf., A* **1996**, *116*, 31−42.
(73) Ruckenstein, E. Effect of Short-range Interactions on Spreading. *J. Colloid Interface Sci.* **1996**, *179*, 136−142.
(74) Ruckenstein, E. Superspreading: A Possible Mechanism. *Colloids Surf., A* **2012**, *412*, 36−37.
(75) Kovalchuk, N. M.; Trybala, A.; Arjmandi-Tash, O.; Starov, V. Surfactant-Enhanced Spreading: Experimental Achievements and Possible Mechanisms. *Adv. Colloid Interface Sci.* **2016**, *233*, 155−160.
(76) Rosen, M. J. Predicting Synergism in Binary Mixtures of Surfactants. *Surfactants and Colloids in the Environment; Steinkopff* **1994**, *95*, 39−47.
(77) Kovalchuk, N.; Trybala, A.; Mahdi, F.; Starov, V. Kinetics of Spreading of Synergetic Surfactant Mixtures in the Case of Partial Wetting. *Colloids Surf., A* **2016**, *505*, 23−28.
(78) Wenzler, L. A.; Moyes, G. L.; Olson, L. G.; Harris, J. M.; Beebe, T. R., Jr. Single-Molecule Bond-Rupture Force Analysis of Interactions Between AFM Tips and Substrates Modified with Organosilanes. *Anal. Chem.* **1997**, *69*, 2855−2861.
(79) Wu, Y.; Rosen, M. J. Synergism in the Spreading of Hydrocarbon−Chain Surfactants on Polyethylene Film − Anionic and Cationic Mixtures by a Two-Step Procedure. *Langmuir* **2005**, *21*, 2342−2348.
(80) Kovalchuk, N. M.; Barton, A.; Trybala, A.; Starov, V. Surfactant Enhanced Spreading: Catanionic Mixture. *Colloid Interface Sci. Comm.* **2014**, *1*, 1−5.
(81) Kovalchuk, N. M.; Barton, A.; Trybala, A.; Starov, V. Mixtures of Catanionic Surfactants Can Be Superspreaders: Comparison with Trisiloxane Superspreader. *J. Colloid Interface Sci.* **2015**, *459*, 250−256.
(82) Kovalchuk, N. M.; Matar, O. K.; Craster, R. V.; Miller, R.; Starov, V. M. The Effect of Adsorption Kinetics on the Rate of Surfactant-Enhanced Spreading. *Soft Matter* **2016**, *12*, 1009−1013.
(83) Marmur, A. Wetting on Hydrophobic Rough Surfaces: To Be Heterogeneous Or Not To Be? *Langmuir* **2003**, *19*, 8343−8348.
(84) Lodge, R. A.; Bhushan, B. Wetting Properties of Human Hair by Means of Dynamic Contact Angle Measurement. *J. Appl. Polym. Sci.* **2006**, *102*, 5255−5265.
(85) Yuan, Y.; Lee, T. R. Contact Angle and Wetting Properties. *Surface Science Techniques*; Springer: Berlin, 2013; pp 3−34.
(86) Molina, R.; Comelles, F.; Julia, M. R.; Erra, P. Chemical Modifications on Human Hair Studied by Means of Contact Angle Determination. *J. Colloid Interface Sci.* **2001**, *237*, 40−46.
(87) Kamath, Y. K.; Dansizer, C. J.; Weigmann, H. D. Wetting Behaviour of Human Hair Fibers. *J. Appl. Polym. Sci.* **1978**, *22*, 2295−2306.
(88) Rungjiratananon, W.; Kanamori, Y.; Nishita, T. Wetting Effects in Hair Simulation. *Computer Graphics Forum* **2012**, *31*, 1993−2002.
(89) Trybala, A.; Bureiko, A.; Kovalchuk, N.; Arjmandi-Tash, O.; Liu, Z.; Starov, V. M. Wetting Properties of Cosmetic Polymeric Solutions on Hair Tresses. *Colloid Interface Sci. Comm.* **2015**, *9*, 12−15.
(90) Feughelman, M. *Mechanical Properties and Structure of Alpha-Keratin Fibres: Wool, Human Hair and Related Fibres*; UNSW Press: Sydney, 1997.
(91) Robbins, C. *Chemical and Physical Behaviour of Human Hair*, 3rd ed.; Springer-Verlag: New York, 1994.
(92) Dupres, V.; Langevin, D.; Guenoun, P.; Checco, A.; Luengo, G.; Leroy, F. Wetting and Electrical Properties of the Human Hair Surface: Delipidation Observed at the Nanoscale. *J. Colloid Interface Sci.* **2007**, *306*, 34−40.
(93) Bureiko, A.; Trybala, A.; Huang, J.; Kovalchuk, N.; Starov, V. M. Bulk and Surface Rheology of Aculyn 22 and Aculyn 33 Polymeric Solutions and Kinetics of Foam Drainage. *Colloids Surf., A* **2013**, *434*, 268−275.
(94) Bureiko, A.; Trybala, A.; Huang, J.; Kovalchuk, N.; Starov, V. M. Effects of Additives on the Foaming Properties of Aculyn 22 and Aculyn 33 Polymeric Solutions. *Colloids Surf., A* **2014**, *460*, 265−271.
(95) Aculyn 22, Technical Data Sheet, Dow http://www.dow.com/assets/attachments/business/pcare/aculyn/aculyn_22/tds/aculyn22.pdf.
(96) Aculyn 33, Technical Data Sheet, Dow http://www.dow.com/assets/attachments/business/pcare/aculyn/aculyn_33/tds/aculyn33.pdf.
(97) Bico, J.; Thiele, U.; Quéré, D. Wetting of Textured Surfaces. *Colloids Surf., A* **2002**, *206*, 41−46.
(98) Bormashenko, E.; Musin, A.; Whyman, G.; Zinigrad, M. Wetting Transitions and Depinning of the Triple Line. *Langmuir* **2012**, *28*, 3460−3464.
(99) Barbieri, L.; Wagner, E.; Hoffmann, P. Water Wetting Transition Parameters of Perfluorinated Substrates with Periodically Distributed Flat-top Microscale Obstacles. *Langmuir* **2007**, *23*, 1723−1734.
(100) Wang, J.; Chen, D. Criteria for Entrapped Gas under a Drop on an Ultrahydrophobic Surface. *Langmuir* **2008**, *24*, 10174−10180.
(101) Velarde, M. G. Honorary note. *Adv. Colloid Interface Sci.* **2007**, *134−135*, 1.

DOI: 10.1021/acs.langmuir.6b04094
Langmuir 2017, 33, 4367−4385